Design of a System to Monitor Youth Workers' Heat Stress and Positioning using Non-invasive Techniques

Matthew Kreisman Kandel

Thesis submitted to the faculty of the Virginia Polytechnic Institute and State University in partial fulfillment of the requirements for the degree of

Master of Science
In
Mechanical Engineering

Bobby Grisso Jr., Co-Chair

Thomas E. Diller, Co-Chair

Alfred L. Wicks

December 7, 2011
Blacksburg, Virginia

Keywords: health, heat exhaustion, proximity, XBee, ZigBee, sensor development, handheld device

Design of a System to Monitor Youth Workers' Heat Stress and Positioning using Non-invasive Techniques

Matthew Kreisman Kandel

Virginia Polytechnic University and State University, 2011
Supervisors: Dr. Robert Grisso, Dr. Tom Diller, Dr. Al Wicks

ABSTRACT

Due to inadequate training and an undeveloped ability to recognize dangerous scenarios, youth workers are exposed to many dangers in the agriculture and lawn care industries. With the abundance of new technologies available on the market, a project was devised to prevent youth from heat exhaustion and equipment run overs by employing sensor based technologies. Using aural temperature measurement techniques involving a thermistor and thermopile, an accurate estimation of core body temperature can be made. The measurements performed by the devices are recorded and transmitted wirelessly over a ZigBee network using XBee radiofrequency modules. Utilizing the properties of radiofrequency transmission, the Received Signal Strength Indication (RSSI) is used to approximate the distance between devices. With accuracy comparable to GPS methods and no necessity for line of sight to sky, RSSI supplies a more than adequate estimate for proximity distance. The temperature and RSSI values are then sent to a coordinating modem where the data is displayed for the supervisor. After testing and calibrating the device, it was found that these methods are effective for the monitoring of core body temperature and proximity of workers. The temperature sensor was able to measure temperatures with less than 0.25% error and the proximity sensor was able to estimate distance within 1.25 meters at close range.

Acknowledgements

A strong thank you goes out to my entire committee for their assistance throughout this project. Requiring subject matters ranging from heat flux measuring to circuit development; their guidance was a necessity to this project, this thesis, and my graduate career. Beginning in August 2010, Dr. Grisso took me onboard with his envisioned project based out of Biological Systems Engineering. Without his vision and project management skills, this project never would have gotten off the ground. Known for his heat flux expertise, Dr. Diller was added to the committee to guide me through the principles in temperature detection and measurement. Dr. Wicks was added shortly thereafter, for his vast knowledge of electronics and signal processing. Each playing a key role in the diverse components of the project, the knowledge supplied by Dr. Grisso, Dr. Diller, and Dr. Wicks was not only a benefit, but a necessity.

I would like to thank the agencies who helped to fund this project. This project never would have fabricated if not for the funding, in part, by the National Youth Farm Safety Education and Certification (Grant No. USDA/NIFA-2010-41521-20830), the National Institute of Food and Agriculture, and the U.S. Department of Agriculture.

Lastly, I would like to thank all of my friends, family, and co-workers who helped both in and out of the lab. Mom and Dad, without your support I can honestly say that I would not be where I am today. A special thanks to John Bird, who took time off from his own research to assist me from beginning to end of the PCB development process. And without the welcomed distractions from my friends, both local and distant, I cannot say that I would have been able to undergo this demanding process. Thank you, all of you.

Table of Contents

Acknowledgements iii

Table of Contents iv

Symbols and Indices vi

List of Figures vii

List of Tables ix

1 Introduction and Motivation 1

2 Background 2

2.1 Heat Stress 2

2.2 Core Body Temperature Measuring Methods 3

2.2.1 Thermistors 4

2.2.2 Infrared Sensors 5

2.3 XBee Modules 7

2.4 Proximity Sensing 8

2.4.1 RSSI 9

3 Experimental Methods 10

3.1 Equipment Setup 10

3.1.1 Thermistor Circuit 10

3.1.2 Infrared Sensor Circuit 12

3.1.3 ZigBee Network Setup 18

4 Testing and Results 20

4.1 Thermistor 20

4.2 Thermopile 22

4.3 RSSI 30

5 Conclusion 32

6 Future Work 33

7 Bibliography 34

8 Appendix A: Thermistor Computer Model 37

9 Appendix B: Eagle PCB Model 39

10 Appendix C: Python Code 41

11 Appendix D: IR Sensor Radiosity Model 46

12 Appendix E: IRB Approval Letter 48

13 Appendix F: IRB Consent Form 50

14 Appendix G: Letters of Permission for Copyright Material 53

Symbols and Indices

Latin letters:

Sign	Unit	Designation
E_b	J	Blackbody Radiation
F	-	Calibration Factor
g	m/s^2	Gravity
G	W/m^2	Irradiation
I	A	Current
J	W/m^2	Radiosity
K	-	Instrument Factor
P	W	Power
q''	W/m^2	Heat Flux
R	Ω	Resistance
t	s	Time
T	K	Temperature
V	V	Volts
W	J	Work
x	m	Distance

Greek letters:

Sign	Unit	Designation
ε	-	Emissivity
Ω	*Ohms*	Resistance
ρ	-	Reflectivity
σ	m^2kg/s^2K	Stefan-Boltzmann constant

List of Figures

Figure 1: Infrared image of an individual both before and after being subjected to fifteen minutes of exercise [13]. 3

Figure 2: Comparison of wavelengths that exists in the electromagnetic spectrum 6

Figure 3: Infrared sensor with the thermopile and thermistor labeled [24] 7

Figure 4: Digi ConnectPort X4 and two XBee RF modules 8

Figure 5: Voltage divider to convert thermistor resistance into voltage 10

Figure 6: Derived relationship between thermistor output voltage and temperature 11

Figure 7: Computer model response of thermistor submerged in water 11

Figure 8: Calibration of thermopiles supplied by PerkinElmer [29] with the TP333 highlighted in blue (device temperature at 25 °C) 12

Figure 9: Difference in temperature between the surface and sensor as a function of voltage 13

Figure 10: Circuit model of TPS 333 thermopile sensor 14

Figure 11: Thermopile circuit containing an In-Amp and several components to eliminate AC signals 14

Figure 12: Figure explaining temperature referencing for the IR sensor 15

Figure 13: Voltage divider circuit for the IR sensor's thermistor 16

Figure 14: Relationship between IR sensor's thermistor resistance and output voltage 17

Figure 15: Printed Circuit Board containing all elements of the thermopile and thermistor circuits 18

Figure 16: Running of program using Telnet and the output of devices involved 19

Figure 17: Thermistor response to being submerged in water at 36.55 °C 20

Figure 18: Thermistor model with volume adjusted for added epoxy 21

Figure 19: Testing setup for IR sensor implementing a high-emissivity aluminum plate regulated by a temperature controller along with the ZigBee network devices and temperature sensor 22

Figure 20: Actual surface temperature compared to the measured surface temperature from the IR sensor 23

Figure 21: Model of setup for the testing of the IR sensor with the aluminum plate 24

Figure 22: Comparison of calibrated data with original data when measuring the aluminum plate 26

Figure 23: Raw and calibrated (adjusted with calibration factor of 0.79) temperatures detected by the sensor in comparison to the aluminum plate temperature at a variety of different temperatures 27

Figure 24: Results measured by the device at different increments while measuring a temperature of 39.1 °C 28

Figure 25 and Figure 26: IR sensor system response showing the outputs of the thermistor and thermopile (adjusted) as the sensor is exposed to the blackbody plate at 41.5 °C at both a 1.5 mm distance and 8 mm distance and adjusted with a calibration factor of 0.83 and 0.61 respectively 29

Figure 27: Diagram of current device design implemented with a human ear 30

Figure 28: Relationship of RSSI to distance for clear both clear and obstructed line of sight 31

List of Tables

Table 1: Table comparing the 63% and 95% rise times for the computer model and experiment results 21

Table 2: Calibration factors for the different distances the IR sensor is from the aluminum plate 28

1 Introduction and Motivation

In the United States, agriculture ranks as one of the most hazardous industries for youth workers. Current regulation and training programs have helped the safety of youth workers, limiting the amount of injuries to less than 1% of the workers. However, when you consider the youth workforce accounts for over 1,000,000 persons in farming alone, this seemingly small percentile correlates with the injuries of 16,851 youth workers and the deaths of 695 others [1]. Considering the most common sources for injuries involved motor vehicles, drowning, machinery, and heat exhaustion, it would seem reasonable to implement new technologies to decrease or even eliminate the possibility of these preventable misfortunes from occurring.

Hyperthermia, more commonly known as heat stress, is defined as the condition when an individual's core body temperature escalates above the body's ideal operating temperature, called the hypothalamic set point, which can result in severe central nervous system dysfunction [2]. When the core temperature rises significantly, heat-related illnesses can occur, which are often fatal, while those that do survive often sustain permanent neurological damage [3]. It has been seen that heat stress is most prevalent in young children and the elderly [4]. With numerous young people working for lawn care, turf management, sod production, and other physically demanding outdoor jobs in Virginian neighborhoods and farms, there is a very relevant risk for these laborers to be at risk of debilitating injury.

In addition to environmental dangers, young workers are at the highest risk for equipment injuries and run-overs, due to inadequate training and minimal experience involved when first starting a new job. Realizing these dangers, the Virginia Cooperative Extension set out to develop a system that would monitor workers relative positions in addition to core body temperature to minimize equipment run-overs in the lawn care and farm management industry as well as monitor for hyperthermia.

2 Background

2.1 Heat Stress

It is common for an individual to undergo hyperthermia while exercising or operating in a hot environment [2, 5]. Hyperthermia is defined as the occasion when the core body temperature rises above the body's ideal operating point, which is set by the preoptic area of the anterior hypothalamus in the brain [2]. This temperature is different for everyone, but the generally accepted value is 37 ± 0.6 °C (98.6 ± 1 °F) [6]. The hypothalamus is the part of the brain that is responsible for monitoring and regulating body temperature. When the hypothalamus detects a body temperature above the set point, it will trigger perspiration and dilate the dermal blood vessels to promote heat dissipation, cooling the subject, and returning the body to the ideal core body temperature [2, 7]. To maintain blood pressure, splanchnic blood flow, blood flow to internal organs, is reduced to compensate for the excess flow of blood to the skin [8].

When the body is subjected to high environmental heat or strenuous physical activity, the body's thermoregulatory responses may be inadequate to preserve homeostasis, or a constant temperature, within the body. This leads to the dangerous aspect of hyperthermia, the uncontrollable increase in core body temperature [9]. The first onset of danger comes in the form of heat exhaustion. Heat exhaustion is defined as a core body temperature above 37 °C (98.6 °F) but less than 40 °C (104 °F) [2]. Thirst, weakness, discomfort, anxiety, dizziness, fainting, and headache are common symptoms that may signify when an individual is in the stage of heat exhaustion [2]. Due to the possibility of fainting and dizziness, heat exhaustion can be dangerous when operating heavy machinery, but there are no direct dangers from the condition itself. When an individual is diagnosed with heat exhaustion, the effects are easily reversible by ingesting nonalcoholic fluids and the separation of the subject from heat sources.

However, when heat exhaustion goes unnoticed it can lead to the most severe and often fatal outcome of heat stress, heat stroke. When the subject's core temperature rises above 40 °C (104 °F), the individual is classified as being in a high state of risk for heat stroke. When a heat stoke occurs the central nervous system breaks down, resulting in delirium, convulsions, or even coma [2]. At this point, damage to the nervous system and loss of organ function is likely and aggressive clinical treatment is required for recovery. It is important to immediately transfer the subject to a cool area and place them in an ice bath. If possible, the victim can administer antipyretic drugs to reduce core body temperature and prevent further damage to the central nervous system.

Although the central nervous system dysfunction that manifests the subject at the time of incident is the distinguishing indicator of a heat stroke, the deteriorating physical health of the victim over the next 48 hours is responsible for the majority of permanent damage. When the body reduces the splanchnic blood flow to maintain blood pressure, linkages connecting digestive organs are weakened and can result in the release of dangerous bacteria and endotoxins into the blood stream [10]. It is commonly found that liver damage accompanies heat stroke and is present within 24 to 48 hours after time of heat exposure [11]. In the case that the liver is severely damaged, the victim's body will be unable to successfully remove

the released endotoxins from circulating the body. These endotoxins cause a condition called disseminated intravascular coagulation (DIC). DIC entails the activation of blood clotting mechanisms which results in the formation of small blood clots inside the blood vessels [12]. These small blood clots consume the coagulation proteins that are required for normal clotting, resulting in abnormal bleeding from the mouth, skin, and internal organs. In addition, the small clots disrupt the flow of blood to bodily organs. Ultimately, these conditions compound the problem, resulting in multiple organ failure and often death.

2.2 Core Body Temperature Measuring Methods

Understanding the severity of heat stroke and the lack of effective treatment methods available, a technique to detect and prevent the condition was proposed. Initially, it was speculated that a simple, low-cost method of monitoring a group of people's body temperature would be to scan the population with an infrared camera. After spending a day operating a FLIR i7 infrared camera to capture images of different subjects in different heat conditions, it was apparent that there would be no accuracy in using this method. The reason for the inaccuracy is based on the infrared camera's limited ability to only observe the surface temperature of objects. As an individual's core temperature increases, the sweat glands on the skin dilate and cool the skin. To the camera, it would appear that the individual is getting colder when in fact their core body temperature is rising [13].

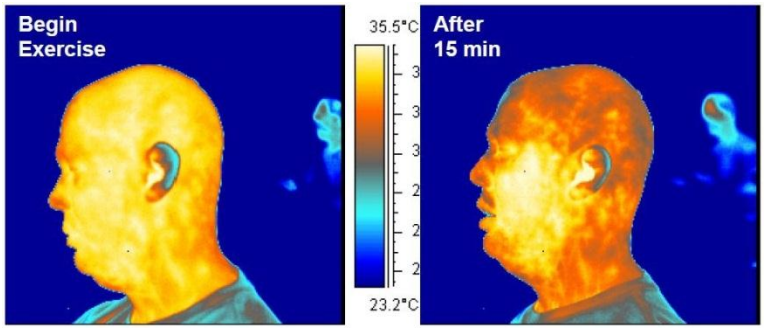

Figure 1: Infrared image of an individual both before and after being subjected to fifteen minutes of exercise [13].

With infrared imaging eliminated, a new solution needed to be derived to monitor core body temperature.

Since measuring the core temperature of a subject requires intrusive techniques, relationships between core body temperature and other body properties were investigated. It was found that there is a strong correlation between heart rate and core body temperature [14, 15]. A linear relationship exists between heart rate and esophageal temperature, regardless of the initial body conditions and environmental conditions.

This relationship between body temperature and heart rate is completely independent of starting body temperature. A second study conducted by Hayashi et al (2006) confirmed that heart rate and core body temperature show a strong correlation, even when subjects wore water perfused suits at different temperatures [14]. Due to the vast technology available and

simplicity for measuring heart rate, the relationship with core body temperature showed promise in making the detection of heat stress both simple and accurate.

Unfortunately, despite the strong correlation between the two, the operating range in which the heart rate is associated with dangerous core temperature levels coincides with moderate levels of physical exertion. A demanding exercise or exhilarating event has the potential to raise an individual's heart rate up to 200 beats per minute [16] independent from the subject's core body temperature. If an individual were to partake in even a moderately physically demanding activity for an extended period of time, it would be impossible to decipher whether the heart rate is increasing from the activity or an increase in core temperature.

It was determined that the most reliable way to determine risk level of heat stress is to measure the core body temperature directly. From a study conducted by Casa et al. [17] on the validity of devices measuring core body temperature, it was found that the rectal thermometer and forehead temperature (when shaded from solar radiation) are the two most accurate measurement methods for measuring core body temperature. These two devices varied from the core temperature by -0.19 °C and -0.14 °C respectively [17]. The third most accurate device was the aural (in-ear) temperature at -1.00 °C. This, however, is slightly larger than the recommended variance of ±0.27 °C, which is the allowable tolerance for medical devices. Since the rectal thermometer is too intrusive for applications in the workplace, the focus was placed on the forehead and aural methods.

The state of the art in medicine uses aural temperature measurement techniques. Easy access to the inner ear which is in close proximity to the hypothalamus, gives a reliable and nonintrusive estimation of what temperature the body is reacting to in its current state. While most workers in agriculture are required to wear hearing protection, it was decided that aural measurements would be the most practical method of monitoring core body temperature.

2.2.1 Thermistors

Thermistors are temperature-sensitive resistors, varying in resistance as a function of temperature. They are easily measurable, small, durable, have a fast response time, and require no temperature referencing. For these reasons, the thermistor was initially chosen for measuring the subject temperature.

Of the temperature transducers, thermistors have one of the fastest response times and are the most sensitive, exhibiting the greatest parameter change with a change in temperature. The relationship between the resistance and temperature can be quantified by either a negative or positive thermal coefficient. The more common NTC (negative thermal coefficient) thermistors have a resistance that decreases as temperature increases [18]. Unfortunately this relationship is non-linear which makes the conversion from resistance to temperature complex.

A well-defined thermistor will be supplied with a list of coefficients (in addition to the resistance at 25 °C) from the manufacturer, which can be used to build the resistance-temperature curve. The most often supplied coefficients are the *A*, *B*, and *C* constants, which are used to develop the Steinhart-Hart equation as seen in equation 1:

$$\frac{1}{T} = A + B\ln R + C(\ln R)^3 \quad (1)$$

where T is the thermistor temperature in kelvin and R is the thermistor resistance in Ohms.

In some instances, a faster computation time may be desired or the manufacturer may only supply a beta parameter, β for an NTC thermistor. In this case, the Steinhart-Hart equation can be simplified to a relationship between the beta parameter, thermistor resistance, and thermistor temperature as seen in equation 2:

$$R = r_\infty e^{\beta/T} \quad (2)$$

where R is the thermistor resistance in ohms, T is the thermistor temperature in kelvin, and r_∞ is the coefficient of decay. Since r_∞ it is a constant, the equation can be solved since the resistance and temperature are known values when the thermistor temperature is at 25 °C:

$$r_\infty = R_{25°C}\, e^{-\beta/T_{25°C}} \quad (3)$$

where $T_{25°C}$ is 298 kelvin. After solving for the coefficient of decay, the equation can be written for temperature as a function of resistance:

$$T = \frac{\beta}{\ln(R/r_\infty)} \quad (4)$$

Aside from the non-linear response, there are several additional disadvantages to working with thermistors. First and foremost, thermistors do not generate their own voltages based on temperature changes. For this reason, they do not require a reference temperature; however, they do require a current source to power the transducer. Based on the amount of current and the size of the resistance within the thermistor, the device may generate heat internally. Since a thermistor is a temperature measuring device, heat generation within the device will be a source of self-heating errors [18]. Fortunately, the amount of heat being introduced to the system can be predicted by using the equation for electrical power:

$$P = I^2 * R \quad (5)$$

where P is the electrical power generated in watts, I is the current running through the thermistor, and R is the resistance of the thermistor. Manufacturers design their products to minimalize the amount of heat generated, however it is useful for modeling purposed to account for this small component.

2.2.2 Infrared Sensors

On the electromagnetic spectrum, infrared (IR) light is the radiation consisting of wavelengths in the range of 0.7 to 300 μm. These wavelengths are longer than visible light radiation, which is perceivable by human vision [19].

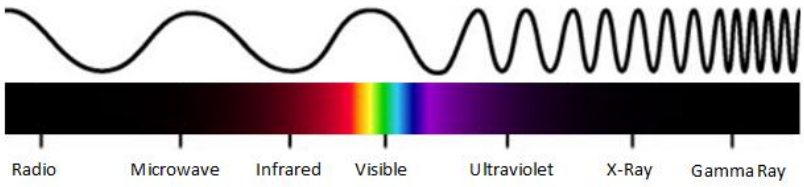

Figure 2: Comparison of wavelengths that exists in the electromagnetic spectrum

Most commonly associated with infrared radiation is heat detection. All objects with a temperature above absolute zero emit thermal radiation, which is a form of electromagnetic radiation that is generated by the thermal motion of the matter's charged particles. For objects such as the sun or a fire, which are very hot, it is easy to perceive the thermal radiation emitted as visible light. These hotter objects (above 480 °C) emit radiation that is within the visible light spectrum. As the temperature of an object decreases, the wavelength of the radiation increases until the point it is no longer visible [20]. Although human vision does not allow us to perceive it, objects at or around room temperature are constantly emitting electromagnetic radiation. The wavelengths for these cooler objects are much longer, placing them in the aforementioned infrared spectrum. In the same way human vision can distinguish radiation in the visual spectrum by associating each wavelength with a distinct color, devices have been produced that correlate this emitted thermal radiation with a temperature.

In the medical field, passive infrared (PIR) sensors are used to accurately detect aural temperatures. By using these passive sensors, the observer is allowed to measure the surface temperature of an object without direct contact to the object itself, a process call pyrometry [21]. PIRs, such as the aural thermometer, make it possible for doctors to take reliable aural temperature measurements, without risking damage to the delicate eardrum. As mentioned before, the eardrum is in close proximity to the hypothalamus, the part of the brain responsible for regulating core body temperature. In essence, a human body will be responding to the temperature of the hypothalamus [17]. For this reason, the eardrum is a desirable indicator of core body temperature, as it will exist at nearly the same temperature as the hypothalamus.

In order for an IR temperature estimation to be accurate, the physical characteristics of the detected object must be known. Emissivity, ε, is a dimensionless quantity that defines how efficiently an objects surface emits energy in comparison to a blackbody [22]. For infrared temperature detection, objects with high emissivity ($\varepsilon > .95$) are desired, as more energy will be detected by the sensor, thus increasing the transducer's resolution. Fortunately, skin has a emissivity of .98, which makes infrared detection a very effective method for body temperature estimation [23].

Several types of transducers are available on the market for measuring infrared radiation. In the medical field, thermoelectric sensors are most commonly implemented. The name "thermoelectric" is derived by the sensors' ability to convert temperature differences into electric voltages. For in-ear detection, the most widely used thermoelectric sensor, the thermopile, is used for nearly all IR temperature measurements.

A thermoelectric infrared sensor implements a thermopile by exposing one end of the sensor towards the surface to be detected and the other end towards an ambient surface. The side of the sensor pointing towards the target surface is equipped with an amplifying lens that gathers the emitted radiation from the surface and focuses it onto the sensor [21]. The barrage of radiation causes the sensor's temperature to rise on the detection side. Meanwhile, the side of the sensor pointing away from the target remains at ambient temperature. This difference in temperature between the two sides of the thermopile results in the generation of a voltage. Knowing the relationship between temperature difference and voltage, the temperature of the target surface can be determined.

Some may have noticed that the above process is leaving out a very important part of determining the object's surface temperature. A thermopile is only capable of determining the temperature *difference* between the detected object's temperature and the ambient temperature. It is not capable of determining the absolute temperature without the use of a reference temperature. Fortunately, most infrared temperature sensors are equipped with a thermistor, which is attached to the enclosure of the device as seen in Figure 3. By using the thermistor to determine the enclosure's (ambient) temperature and the thermopile to determine the difference in temperature between the surface and ambient, the temperature of the target surface can be determined.

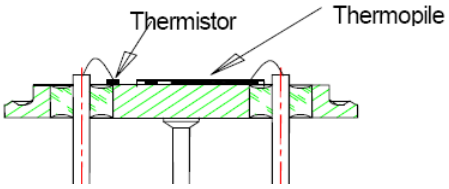

Figure 3: Infrared sensor with the thermopile and thermistor labeled [24]

2.3 XBee Modules

At the commencement of the project, XBee radio frequency modules were recommended as a simple way to transmit information wirelessly. A starter kit was acquired from Digi International [25], consisting of a ConnectPort X4 and several XBee modules (seen in Figure 4). The devices communicate via the ZigBee communication protocol. The protocol is structured so that a coordinator (the ConnectPort X4) communicates with several end devices (XBee modules). XBee modules are radio frequency transmitters that are capable of measuring analog voltages and determining proximity information. When pinged (called) by the coordinator, these end devices send their collected information back to the coordinator to be presented to the supervisor. In addition to the ability to transmit data, the XBee modules are able to relay data from other XBee modules to the modem. In the event that an XBee module moves out of range of the coordinator, the data may still reach the coordinator by relaying the information across other end devices.

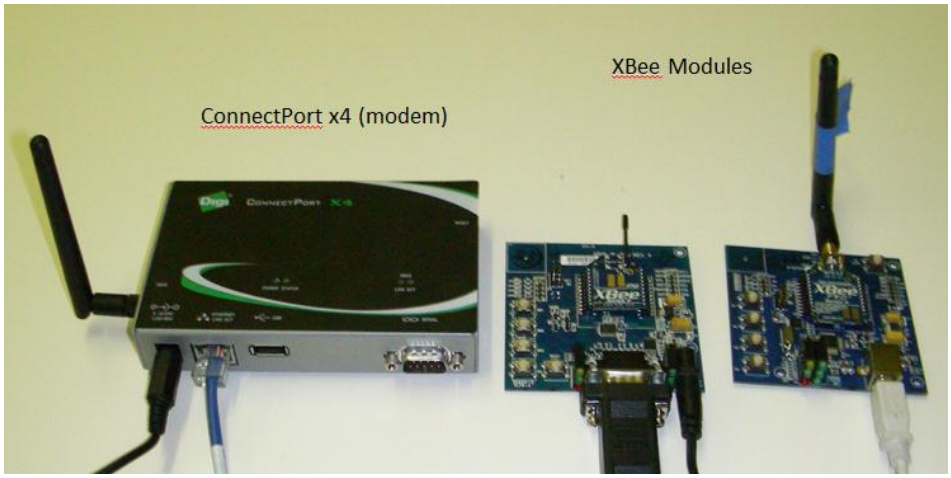

Figure 4: Digi ConnectPort X4 and two XBee RF modules

The XBee module is the central part of each individual's temperature and proximity measuring device. Not only will it measure the voltages of the thermopile and thermistor, but it will also supply the power to the devices and any amplifiers they require. Using this method, an XBee module will be required for each individual being supervised. After collecting the relevant information, the XBee modules will send the raw voltage values to the modem for publishing. It is important to note that these modules are limited to measuring voltages in the range of 0 to 1.2 volts. With a 10 Bit resolution capability on the XBee module, it can be calculated that the device is capable of measuring analog voltages with a resolution of 1.173 mV.

The ConnectPort modem will be running a preprogrammed loop to collect the data. The code (shown in Appendix C) begins by determining which XBee modules are relevant, and names each module with a device number. Next, a loop is initiated in which it calls each module, one at a time, and receives the raw voltage data. The program uses the formulas and calibrations discussed to convert the voltages into temperatures. Next, the temperature values are compared with the critical temperature value (39.5 °C). If the temperature exceeds this critical temperature, the subject is at risk of heat stroke and a warning is produced on the output screen. This process is continued for each device. After all devices are called, converted, and checked, the loop repeats. The ConnectPort is also responsible for creating a display where all devices, temperature values, and any necessary warnings are displayed on a command prompt screen for a supervisor to monitor.

2.4 Proximity Sensing

Motor vehicles accidents account for 18% of injuries and 17% of fatalities among youth workers in agriculture [1]. A study in 2007, found that 16,200 children under the age of 19 were treated by doctors with injuries from lawn mower accidents alone [26]. Through proper training most of these accidents can be avoided, however equipment run overs still pose a threat to inexperienced crew members or observers. With the recent rise in the implementation of sensor based technologies in everyday devices, it seems reasonable that equipment run overs can be prevented.

2.4.1 RSSI

A common property of all radio frequency devices is the ability to detect the received signal strength of a signal. Since this project uses XBee radio frequency transmitters, received signal strength indication (RSSI) is an easily accessed parameter. RSSI is a value that represents how much power is present in a received radio signal. This property is used every day while trying to search for reception on a cellular phone. The bars on the phone are a visual representation of the RSSI the device is able to receive. As the phone moves closer to a cellular tower, the RSSI improves and the cell phone displays more bars.

In addition to simply indicating connection properties, projects have implemented this value to control the positioning of autonomous vehicles [27]. Using the same principles and a well-defined relationship, RSSI can be useful in estimating distance between devices.

Most devices do not use RSSI to estimate distance due to the many factors that can alter the results. In order for RSSI to be completely accurate, line of sight must be established between the devices involved. Any obstructions (e.g., buildings, vehicles, large plants) will diminish the RSSI value and cause the distance between the devices to appear larger than the actual distance. In addition, the atmosphere can influence the signal's path. Primarily occurring in indoor applications, the signal may not take a direct path from the transmitter to the receiver and instead reflect off of walls, ceilings, and furniture on its journey to the end location. This phenomenon is referred to as multipath. In this instance, the distance between the devices would appear larger as well. An estimated distance that is larger than the actual would be extremely ineffective in the prevention of equipment run overs.

Fortunately, these inaccuracies can be overlooked. In the event that a large obstruction is forcing error in the distance estimation, a run over would be improbable as the obstruction itself would shield the two individuals from colliding. As for multipath error, it should be assumed that the vehicle operators have had substantial enough training to know not to operate the vehicles indoors. In outdoor operations, multipath error is only evident at large distances and is almost non-existent for close proximity communications.

3 Experimental Methods

3.1 Equipment Setup

To ensure reliable results, a firm understanding of the methods used to acquire the data is necessary. In this section, the measurement techniques used for each device are explained in detail.

3.1.1 Thermistor Circuit

Recalling how a thermistor operates from the literature review, its thermoelectric properties can be used to detect an object's temperature. Using XBee modules to measure and broadcast the temperature data, the thermistor must be conditioned accordingly. The XBee modules can receive an analog voltage input in the range of 0 to 1.2 Volts. To generate a voltage from a resistive element, the voltage divider seen in Figure 5 was created.

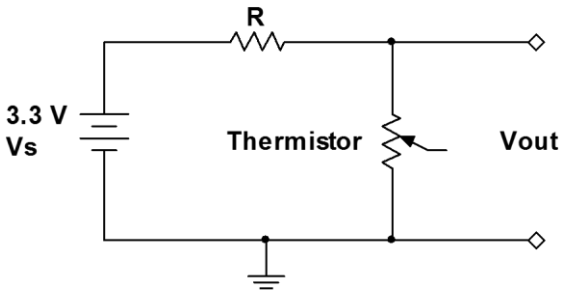

Figure 5: Voltage divider to convert thermistor resistance into voltage

Since the temperature operating range is between 35 °C to 40 °C, a resistive value must be chosen that will allow the full range of temperatures to be measured without exceeding the modules input range of 0 to 1.2 Volts. From the definition of a resistive voltage divider, the equation can be used to derive the size of the resistor required.

$$V_{out} = \frac{V_S R_T}{R + R_T} \quad (6)$$

where R_T is the resistance of the thermistor, V_s is the voltage source, and R is the resistor in question. The voltage source is powered directly from the XBee module's power supply, and is regulated at 3.3 V. Using equation 2 and the Steinhart-Hart equation (equation 1), the expected minimum and maximum values of the thermistor's resistance can be calculated and are 16 kΩ and 20 kΩ for 40 °C and 35 °C, respectively. Using these values along with equation 6, a 100 kΩ resistor was chosen. To verify, a plot of output voltage as a function of temperature was simulated in Figure 6 from the Steinhart-Hart equation, equation 1, and the voltage divider equation, equation 6.

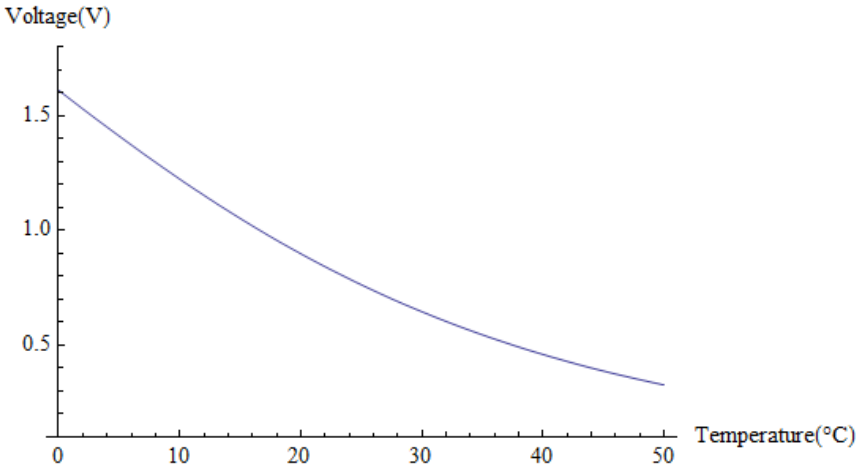

Figure 6: Derived relationship between thermistor output voltage and temperature

It is verified that the range of temperatures for body temperature detection are within the bounds of the analog input the XBee module can detect. Although the resolution is not optimized by a 100 kΩ resistor, this tolerance will allow us to better characterize the system during testing.

For comparison and validation later in the project, a computer model was constructed using Mathematica [28] to simulate the thermistor being submerged into water at a temperature at 36.5 °C. The code for the model can be seen in Appendix A. The predicted response of the thermistor can be seen in Figure 7.

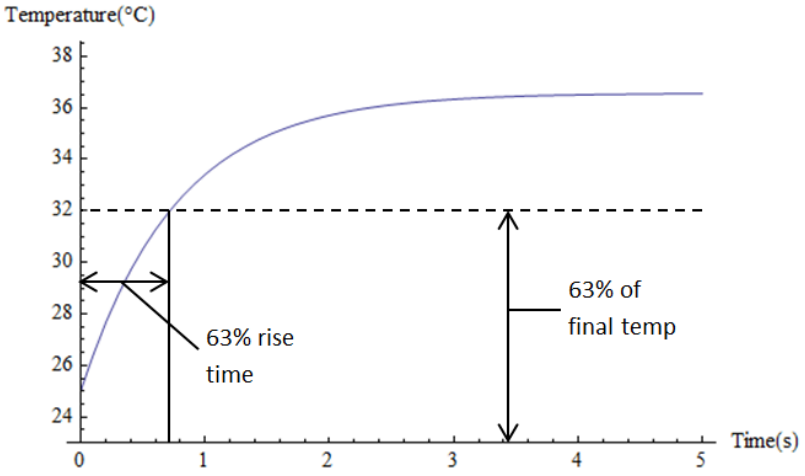

Figure 7: Computer model response of thermistor submerged in water

From the model, the prediction showed a time constant of 0.71 seconds. In other words, it will take 0.71 second for the thermistor to reach 63% of its final (asymptotic) value. Furthermore, it will take 2.24 seconds to reach 95% of the final temperature. Since water has a considerably larger convective heat transfer coefficient than that of air, it would be expected that the response time of the device will be significantly slower for taking

measurements in the ear canal. For verification and validation purposed, the water model will allow us to determine if the thermistor and XBee system is working properly.

3.1.2 Infrared Sensor Circuit

Inspired by aural thermometers, an infrared temperature sensor was developed. The IR sensor consists of a thermistor and a thermopile that work in conjunction to estimate the temperature of the surface in the field of view. In order for the sensor to work effectively, it requires that both the thermistor and thermopile signals are conditioned and measured separately. For the thermistor, the methods used in the Thermistor Circuit section will be repeated, and therefor will not be discussed in detail.

The thermopile is responsible for detecting the difference in temperature between the surface in the field of view and the device itself. To achieve this, the radiation being emitted by the surface in question reaches the device, passes through a longpass infrared filter, and heats up an array of thermocouples inside the device. At this temperature range (35 °C – 40 °C), the voltage outputs are extremely low. A datasheet showing the temperature to output voltage relationship was acquired from the manufacturer, PerkinElmer [29], and can be seen in Figure 8. It should be noted that the calibration curve shown is for a device temperature of 25 °C.

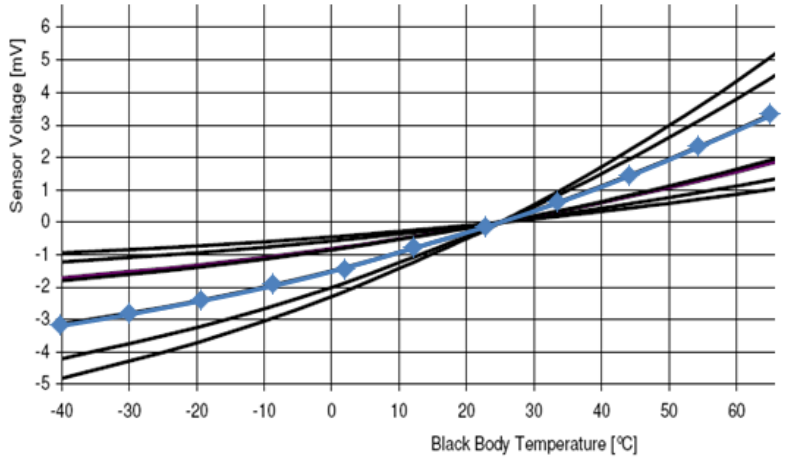

Figure 8: Calibration of thermopiles supplied by PerkinElmer [29] with the TP333 highlighted in blue (device temperature at 25 °C)

Since the device will be measuring voltage to calculate the difference in temperature from the sensor and the surface, the data points seen in Figure 8 were inverted, so temperature could be determined as a function of voltage. In Figure 9, the data points are inverted and a fourth-order best fit curve applied comparing the temperature difference between the surface and sensor as a function of voltage:

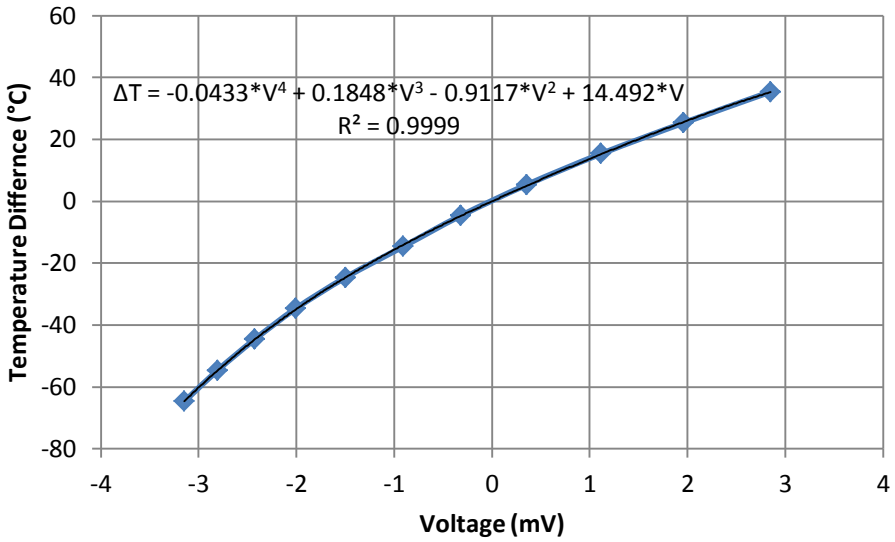

Figure 9: Difference in temperature between the surface and sensor as a function of voltage

with the best fit curve (R^2=0.9999) represented in equation 7:

$$\Delta T = -0.0433 * {V_{pile}}^4 + 0.1848 * {V_{pile}}^3 - 0.9117 * {V_{pile}}^2 + 14.492 * V_{pile} \quad (7)$$

where ΔT is the difference in surface temperature ($T_{surface}$) and sensor temperature (T_{sensor}) and V is the output voltage of the thermopile. It may be noticed that the offset of 24.611 °C in the best fit curve was removed for equation 7. Since the difference of the temperatures is plotted, the 25 °C offset from Figure 8 is removed. A fourth-order fit is justified due to the fourth-order relationship between heat flux and temperature.

With a ΔT range of 0 °C to 10 °C (represented in Figure 8 by a black body temperature of 25 °C to 35 °C), a voltage output range of approximately 0.5 to 1.0 mV is expected. Recalling that the XBee module can only measure voltages ranging from 0 to 1.2 volts with a resolution of 1.173 mV, an amplifier must be implemented. Before developing an amplification circuit, a model was developed to understand the behavior of the thermopile. From the datasheet and a few simple tests, it was found that the thermopile emits a DC voltage signal with a minute amount of AC noise and has an internal resistance of 75 kΩ [30]. The circuit model of the thermopile can be seen in Figure 10.

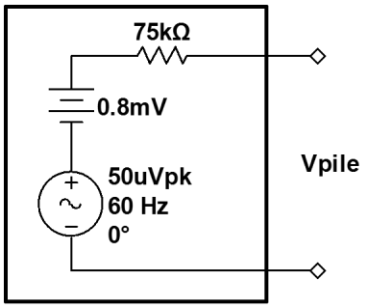

Figure 10: Circuit model of TPS 333 thermopile sensor

To amplify the voltage emitted by the thermopile into the range required for the XBee, a gain of 1200x must be applied to the signal. Applying such a considerable amount of amplification to the signal arises several problems. First any noise present in the signal will be amplified 1200 times. To maintain an acceptable signal to noise ratio, filters and noise eliminating techniques must be implemented to the circuit. Second, tolerances in the circuit components must be minimized. Even small inconsistencies in resistance values can result in large errors when amplifying by such a large magnitude.

To help eliminate the noise problem, an instrumentation amplifier (In-Amp) was utilized to amplify the thermopile signal. An In-Amp, as opposed to an Op-Amp (operational amplifier), has the ability to amplify the difference between the two input voltages without amplifying any fluctuations the signals may be subjected to. This is a significant component in the circuit, as it eliminates any noise the thermopile may contain from environmental interferences as well as amplify the signal to the appropriate voltage range. In addition to the differential amplifier, low-pass filtering techniques can also be employed. Since measuring temperature does not require transient analysis, all AC (alternating current) elements of the signal can be eliminated. Utilizing the methods aforementioned, Figure 11 shows the schematic of the finalized signal condition circuit used for the thermopile.

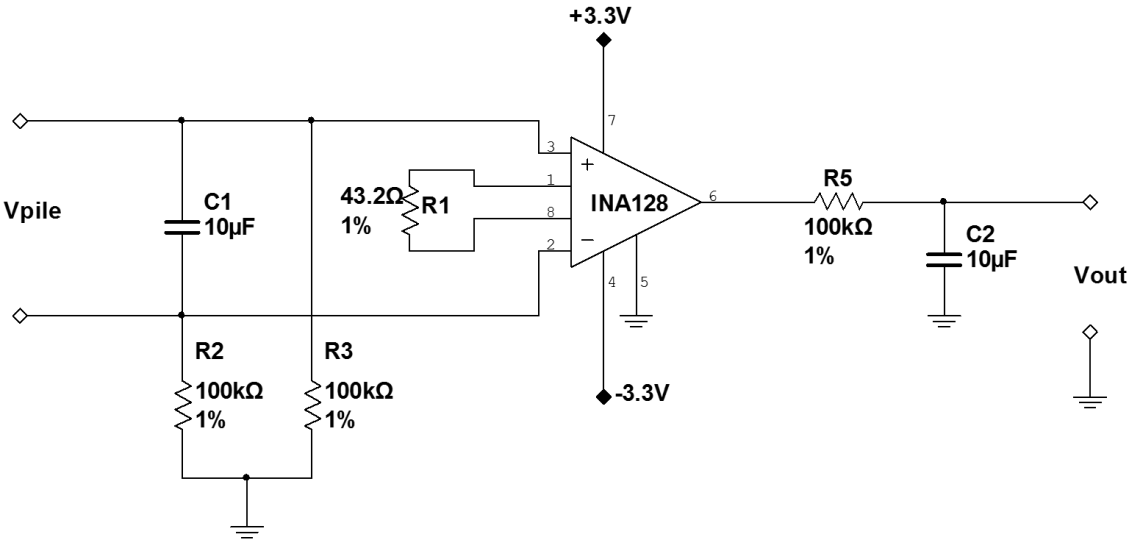

Figure 11: Thermopile circuit containing an In-Amp and several components to eliminate AC signals

As the voltage is sent from the thermopile it enters the circuit on the left, and the first stage of filtering occurs. As capacitor C1 joins the two leads, it will work with the internal resistance of the thermopile and create a low-pass filter. Using equation 8, the cutoff frequency (f_c) of the filter in place can be calculated:

$$f_c = \frac{1}{2\pi RC} \quad (8)$$

Using an internal resistance of 75 kΩ and the 10 μF capacitor, it can be calculated that the filter will only pass components of the signal operating below the cutoff frequency of 0.212 Hz. This means that the values are correct, and only the DC component of the voltage signal should make it to the amplification process.

The INA128 instrumentation amplifier from Texas Instruments [31] was chosen as the device to administer amplification. Specified in its datasheet, it is made for applications involving thermocouple amplification and medical instrumentation, which is appropriate for this project's applications. Since it is a differential amplifier, it takes the difference between the two inputs, amplifies them by a magnitude set by resistor R1, and outputs the voltage in reference to pin 5. Since the temperature referencing involving the thermistor will be performed by the software, the reference is attached to the ground pin.

As the amplified voltage exits the In-Amp, it then passes through a second low-pass filter involving resistor R5 and capacitor C2. Going back to equation 8, it is found that the cutoff frequency of this filter is 0.159 Hz, once again only allowing the DC component of the signal to pass and thus completing the signal conditioning of the thermopile sensor.

The second component of the infrared sensor is the thermistor. Since the thermopile is only capable of detecting temperature differences, a thermistor must supply the reference temperature. A visualization of the process can be seen in Figure 12.

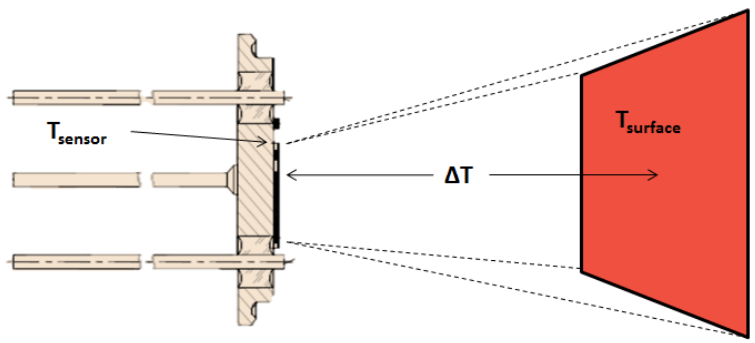

Figure 12: Figure explaining temperature referencing for the IR sensor

It should now be obvious that in order to estimate the surface temperature, the sensor temperature found by the thermistor must be added to the temperature difference detected by the thermopile, as seen in equation 9.

$$T_{surface} = T_{sensor} + \Delta T \quad (9)$$

Using the voltage divider circuit developed in Figure 5 and equation 6, the circuit seen below in Figure 13 was devised to allow an output in the ranges determined by the XBee module's specifications. From the TPS333 infrared sensor datasheet, it was found that the thermistor held a 25 °C resistance of 100 kΩ, which is important in determining the size of the other resistor in the voltage divider.

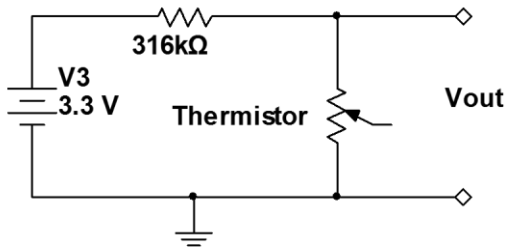

Figure 13: Voltage divider circuit for the IR sensor's thermistor

The thermistor onboard the infrared sensor came with a beta value of 3964 K. This means that equation 2 is necessary to predict the resistance values of the thermistor. Using the values from the datasheet, equation 2 is rewritten:

$$R_T = 0.1682 * e^{3964/T} \quad (10)$$

It is found that the expected minimum and maximum values of the thermistor's resistance are 53 kΩ and 65 kΩ for 40 °C and 35 °C respectively. Using the voltage divider equation, equation 6, along with the calibration equation, equation 10, the following relationship between temperature and output voltage is derived as:

$$V_{out,thermistor} = \frac{3.3V * R_T}{316k\Omega + R_T} = 3.3V * 0.1682 * e^{3964/T_{sensor}-273.15} \Big/ 316k\Omega + 0.1682 * e^{3964/T_{sensor}-273.15} \quad (11)$$

where V_{out} is the output voltage of the thermistor circuit in volts and T_{sensor} is the temperature of the thermistor in degrees Celsius. To visualize the outputs expected in the temperature range the device will be operating in, a plot of output voltage as a function of temperature can be seen in Figure 14.

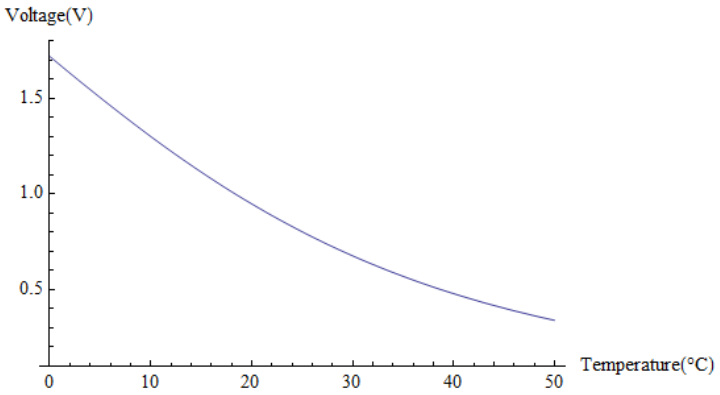

Figure 14: Relationship between IR sensor's thermistor resistance and output voltage

It is validated that the circuit will behave correctly, and will supply an output within the XBee's measurable range of 0 to 1.2 Volts for all temperatures in the expected operating range. Solving equation 11 for temperature as a function of output voltage gives us equation 12.

$$T_{sensor} = 3964 \div \ln\left(\frac{V*316\ k\Omega}{3.3\ V-V} \Big/ 0.1682\right) \quad (12)$$

Using the equations derived from the thermopile and thermistor circuits, and the relationship from equation 9, a final solution can be created. Relating the output voltages of the thermistor and thermopile circuits, the following equation can be stated:

$$T_{surface} = T_{sensor} + \Delta T \quad (13)$$

$$T_{sensor} = 3964 \div \ln\left(\frac{V*316\ k\Omega}{3.3\ V-V} \Big/ 0.1682\right) \quad (14)$$

$$\Delta T = -0.0433 * {V_{pile}}^4 + 0.1848 * {V_{pile}}^3 - 0.9117 * {V_{pile}}^2 + 14.492 * V_{pile} \quad (15)$$

Using the method of software temperature referencing does have its disadvantages. For one, it requires two separate measurements, one for the thermistor voltage and the other for the thermopile voltage. Second, due to hardware limitations, if the surface temperature is below the sensor temperature, the detected surface temperature will be that of the sensor temperature. Since the XBee modules can only read voltages in the range of 0 to 1.2 Volts, any negative temperature difference will be recorded as a voltage of zero. This is acceptable for the project application, as in the event the device temperature is higher than the object temperature, a warning will still be displayed if the temperature is above the critical threshold.

To maintain that the device remains portable, an extra step was added to the project to develop a printed circuit board (PCB). Using EAGLE PCB design software [32], a model of

the circuit was created and a PCB the size of the XBee module was constructed, as seen in Figure 15. A detailed explanation of the steps in the PCB design process can be found in Appendix B.

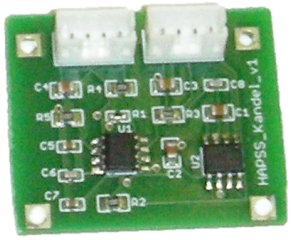

Figure 15: Printed Circuit Board containing all elements of the thermopile and thermistor circuits

3.1.3 ZigBee Network Setup

Even though XBee modules are designed to be easily implemented into projects, there are some techniques required to enable the ZigBee network to function correctly. To program the coding and communicate with the coordinator (ConnectPort X4), a customized version of the Python programming language was used, called Digi ESP for Python [33]. The program was optimized to run with the ZigBee network.

After giving the coordinator an IP address and setting it to communicate with the end devices via their MAC addresses, an inline code must be created to tell the system how to operate. The inline code used for this project can be found in Appendix C. In the coding, it is declared which analog input pins to sample and at what sampling rate. Then using the equation derived in the previous sections, the temperature is calculated from the sampled analog voltages. Finally, the code prints the relevant information, allowing the supervisor to view the temperature and proximity information and any warnings present.

When the code is executed using Digi ESP for Python, all script files necessary for running the program are sent to the coordinator. Here the coordinator runs the code and pings (verifies a communication with) each XBee module one at a time. When the connection is acknowledged, the XBee sends the requested information back to the coordinator. The coordinator then sends the received data through the calculations and prints the information on the network. The coordinator then pings the next device, and the process is repeated indefinitely until the program is terminated.

After the initial execution of the code, the files remain with the coordinator. By establishing a Telnet with the coordinator, the program can be run by a computer without Digi ESP for Python. The Telnet will open the command prompt window, where the program can be initialized and ran. All outputs from the code will appear, with proper format, in the command prompt window. An example of the output can be seen below in Figure 16.

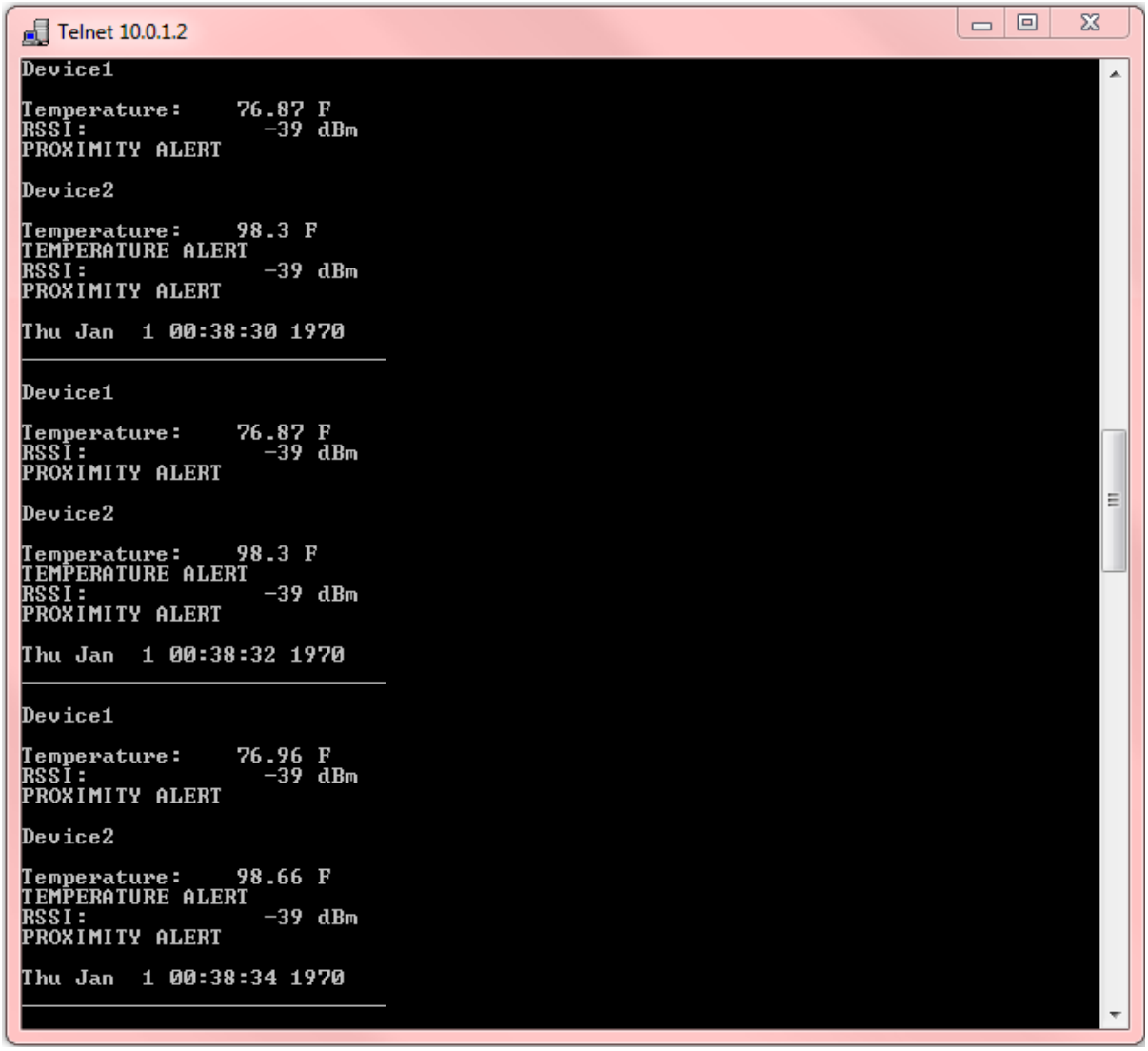

Figure 16: Running of program using Telnet and the output of devices involved

4 Testing and Results

4.1 Thermistor

The first test conducted was submerging the thermistor into water, and comparing the response to the model constructed in the previous section. This will not only verify that the thermistor is behaving correctly, but also verify that the XBee modules are operating properly.

To conduct the experiment a Dewar flask, a highly-insulated container, was filled with heated water and stirred, to make the temperature profile of the fluid uniform. An RTD (resistance temperature detector) with a platinum resistance probe was used to monitor the temperature of the water as it reached steady state in the Dewar flask. The water settled at a temperature of 36.55 °C, which is approximately the average human core body temperature.

After the water settled to a steady temperature and the temperature profile of the fluid was uniform, the thermistor was submerged and the temperatures recorded. A plot of the results as well as the 63%, 95%, and water temperature were constructed in Figure 17.

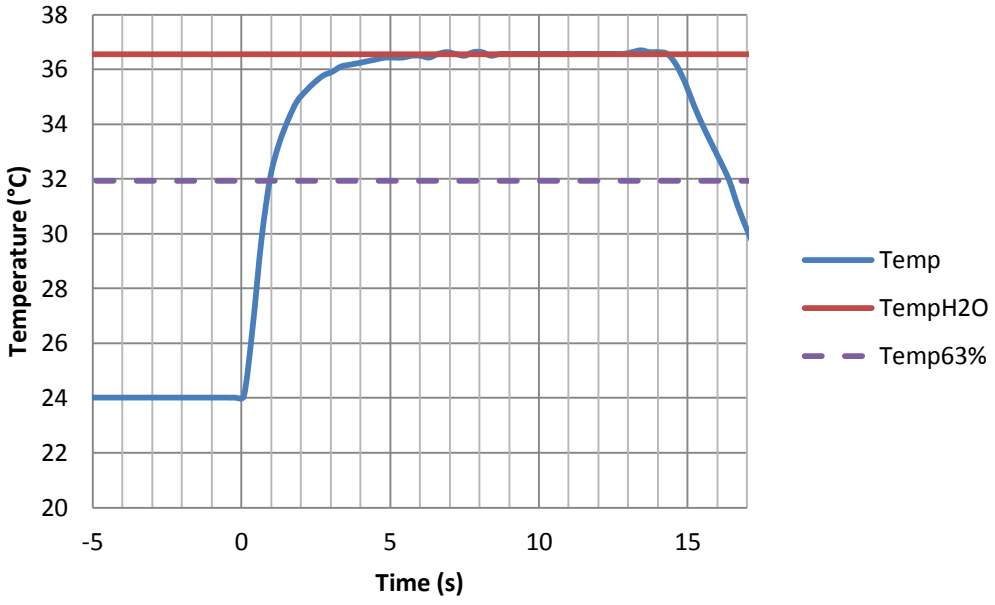

Figure 17: Thermistor response to being submerged in water at 36.55 °C

From the experiment, it was found that the time required for the thermistor to reach 63% of the final temperature is 0.97 seconds. After 3.04 seconds, the thermistor reaches 95% of the final temperature and continues to settle appropriately. At the 14 second mark, the thermistor is removed from the water bath. The temperature then quickly decreases from evaporation.

Recalling the computer model predictions, the expected values with the measured values are compared in Table 1.

Table 1: Table comparing the 63% and 95% rise times for the computer model and experiment results

Method	63% of Final Temp (s)	95% of Final Temp (s)
Computer Model	0.71	2.24
Experiment Results	0.97	3.04

It is seen that the experimental response times are slightly longer than the predicted values. This can be attributed a layer of epoxy added to the thermistor to make the device water proof. The added layer of epoxy will increase the thermal resistance of the device and explains why the time constant in the experiment is longer than expected.

With the source of inconsistency identified, the model can be modified by adjusting the volume to accommodate the added epoxy.

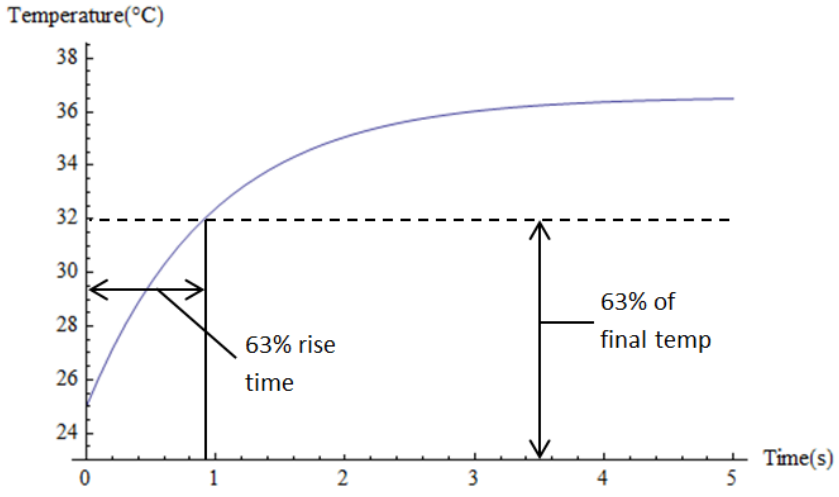

Figure 18: Thermistor model with volume adjusted for added epoxy

It is seen from the graph that by accounting for the added volume the epoxy creates, the experiment is operating with only a 2.1% error. The 0.95 second time constant from the adjusted model verified that the thermistor is behaving as expected. It can also be deduced that the XBee module is working correctly as well. With the response characterized almost perfectly by the computer model, it is apparent that the XBee is measuring the voltage values and converting them to temperature correctly and promptly. This will supply confidence in calibrating and testing the IR sensor. Any errors in the future can be attributed to the device and calibration formulas rather than the measurement abilities of the XBee module.

4.2 Thermopile

Calibration of the thermopile was more involved. In order to produce a measurable and predictable temperature, an aluminum plate painted with Zynolyte® Hi-Temp Paint enamel. The enamel supplies a highly emissive surface to the aluminum plate allowing the plate to serve as a near blackbody. Embedded in the plate, are several thermocouples along with a heating element. By connecting a thermocouple and the heating element to the controller, the temperature of the aluminum plate can be accurately regulated and monitored via a display located on the controller. The test setup can be seen in Figure 19.

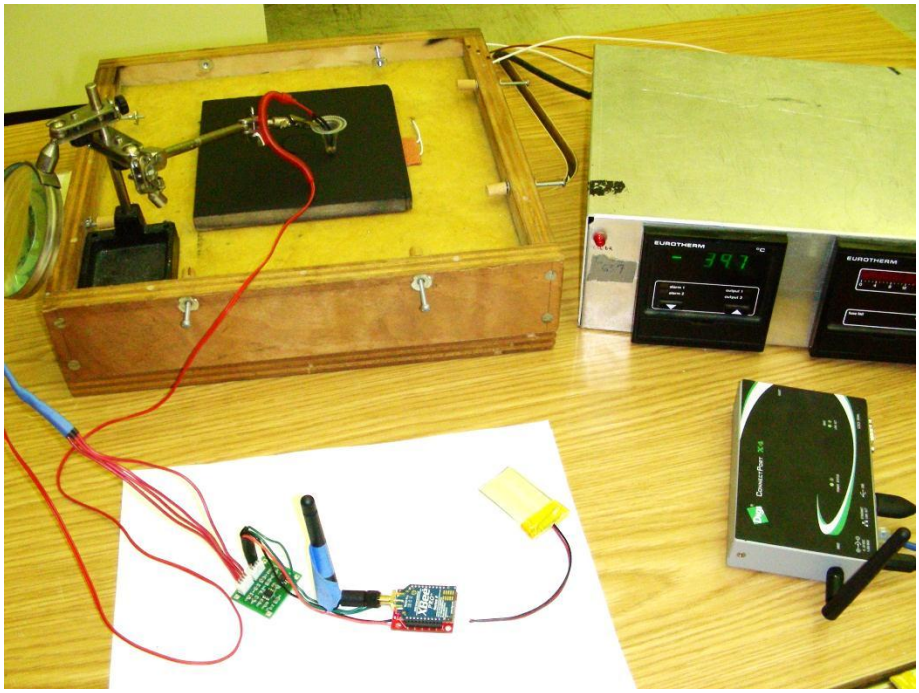

Figure 19: Testing setup for IR sensor implementing a high-emissivity aluminum plate regulated by a temperature controller along with the ZigBee network devices and temperature sensor

Also pictured is the XBee module and ConnectPort X4. The XBee module is attached to a 3.7 Volt battery and the signal conditioning PCB, discussed earlier. The IR sensor is connected to the signal conditioning PCB as well, and the sensor end is suspended from a clamp above the aluminum plate at a height of 5 mm, and the sensor was pointed directly down at the surface.

Steps were taken to calibrate the test setup to ensure that the surface temperature being measured was accurate. Since the controller is responsible for regulating and displaying the aluminum plate's temperature, the temperature displayed by the controller was tested for accuracy. First, a separate thermocouple, one not embedded in the aluminum plate, was connected to the controller. The thermocouple was then submerged into a Dewar flask filled with water. The output temperature of the controller was compared with a mercury thermometer, accurate up to 0.02 °C. It was found that controller had an offset of +0.4 °C, meaning that the actual temperature of the aluminum plate is 0.4 °C less than the displayed temperature on the controller. This offset is accounted for in all results seen in this paper.

The first test administered for the IR sensor involved setting the aluminum plate to 39.1 °C and recording the surface temperature for several hours. The distance between the sensor and the surface was 3.2 mm. This revealed any calibration methods required, as well as any errors in the device that may arise over extended durations. A graph of the surface temperature sensed by the device compared to the actual surface temperature is seen in Figure 20.

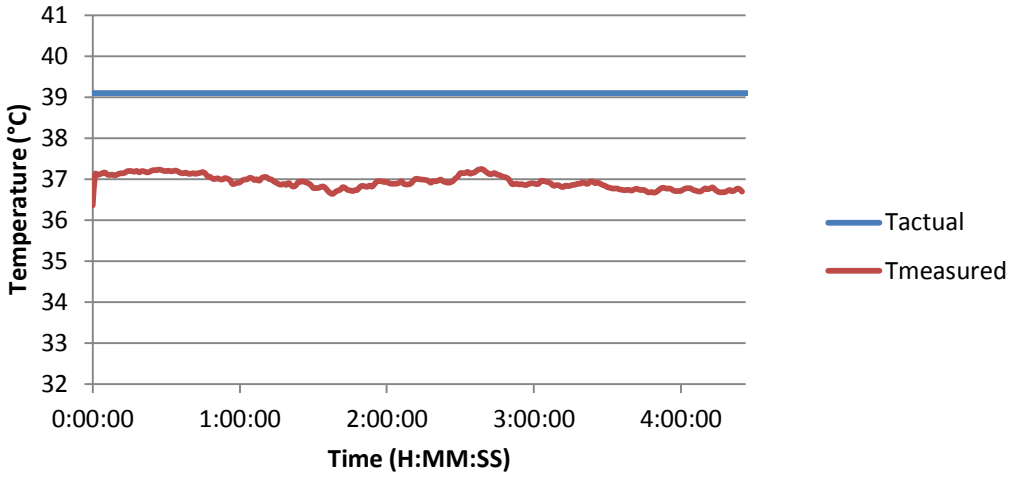

Figure 20: Actual surface temperature compared to the measured surface temperature from the IR sensor

From the test the IR sensor estimated a temperature of 2.17 °C lower than the actual, on average, at 39.1 °C. On the positive note, there is no drifting of the values over the four hour testing duration. So it seems that the equations derived earlier are missing a crucial step in using infrared radiation to predict temperature.

Although the surface being measured was painted with a high-emissivity flat black paint, it cannot be assumed to be a blackbody. While a blackbody has an emissivity of 1 (definition of a blackbody), the paint used to coat the aluminum plate has an emissivity of approximately 0.98. So rather than a blackbody, the aluminum plate is acting as a gray surface. This indicates that the radiation reaching the sensor is not only radiation emitted from the surface, but also radiation emitted throughout the room that is reflected off of the surface.

By developing a model to characterize the elements of heat-transfer occurring, the sensor can be calibrated to account for the effects. The model, seen in Figure 21, shows the orientation in which the test was administered and the sources of radiation. A detailed explanation of all equations and assumptions can be found in Appendix D.

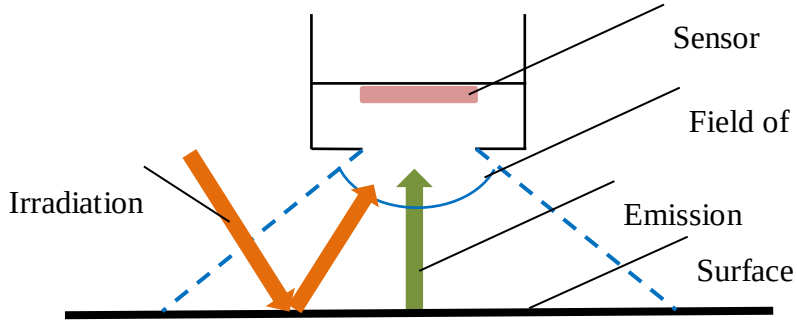

Figure 21: Model of setup for the testing of the IR sensor with the aluminum plate

With the ambient room, there is a significant area on the surface in which irradiation can reflect, and be misinterpreted by the sensor. To characterize this effect, the radiosity, sum of reflected and emitted radiation, is derived in equation 16:

$$J = \varepsilon E_b + \rho G \quad (16)$$

where J is the radiosity of the surface, ε is the emissivity of the surface, $E_{b,surface}$ is the blackbody emissive power of the surface, ρ is the reflectivity of the surface, and G is the irradiation from the room. To make this equation specific to the test setup used, the following relationships are employed. Using these assumptions and definitions the equation can be rewritten as:

$$J = \varepsilon\sigma T_{surface}^4 + (1-\varepsilon)E_{b,room} \quad (17)$$

where σ is the Boltzmann constant, ε is the emissivity of the surface, and $E_{b,room}$ is the blackbody emissive power of the room.

Next, the heat flux equation of the sensor is defined in terms of energy into the sensor and energy out of the sensor:

$$q" = K * J - K * E_{b,sensor} = K\left[J - E_{b,sensor}\right] \quad (18)$$

where $q"$ is the heat flux of the sensor, J is the radiosity of the surface, and $E_{b,sensor}$ is the blackbody emissive power of the sensor. An instrument factor, K, is also added to the equation which will account for any effects from view angle, optical path, and spectral range of the sensor. It should be noted that the radiosity of the surface accounts for the energy going into the sensor and the emissive power of the sensor accounts for energy leaving the sensor. When equation 17 is substituted into equation 18 the following equation is derived:

$$q" = K\left[\varepsilon\sigma T_{surface}^4 + (1-\varepsilon)E_{b,room} - E_{b,sensor}\right] \quad (19)$$

To simplify this expression further, the assumption must be made that the temperature of the sensor is the same as the temperature of the room. After making this assumption, the equation is resolved to:

$$q" = K * \varepsilon\left[\sigma T_{surface}^4 - \sigma T_{sensor}^4\right] \quad (20)$$

Since ΔT is the primary focus, it can be declared that:

$$\Delta T \sim {q"}/{K * \varepsilon} \sim {q"}/{F} \quad (21)$$

where *q"* is the heat flux of the sensor, which is measured by the thermopile, and F is a calibration factor that accounts for all instrumental effects as well as the emissivity of the surface. The calibration factor will be derived experimentally later in the report. From this method, it can be derived that the heat flux measured by the sensor must be divided by the calibration factor. Equation 22 shows how this calibration factor will be applied to the system.

$$T_{surface} = T_{sensor} + {\Delta T}/{F} \quad (22)$$

where $T_{surface}$ is the temperature of the surface being measured, T_{sensor} is the temperature of the sensor (measured by the thermistor), and ΔT is the difference in temperature between the surface and the sensor (measured by the thermopile).

To determine the calibration factor value, the data collected earlier at 39.1 °C was adjusted accordingly until the measured temperature best matched the actual temperature. It was found that a correction factor of 0.79 results in the closest match. The data was corrected by dividing the detected thermopile temperature by the calibration factor, with the results shown in Figure 22.

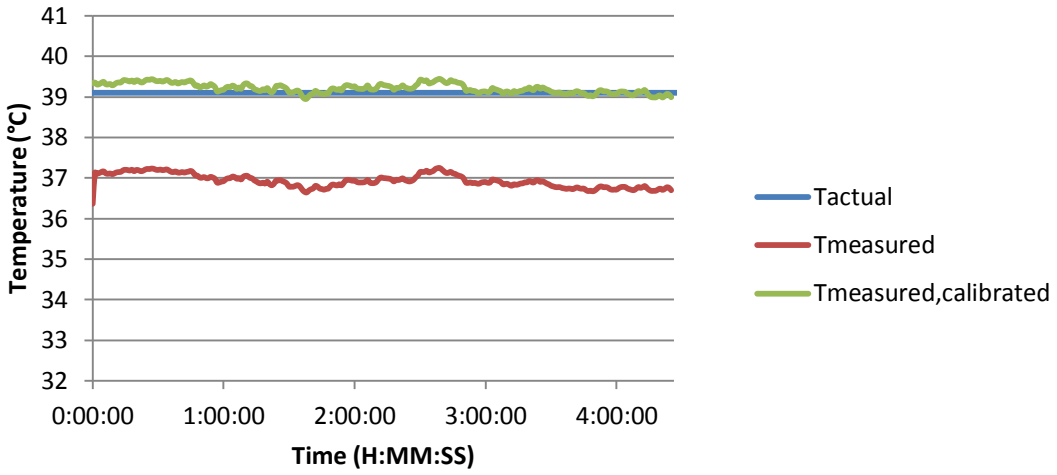

Figure 22: Comparison of calibrated data with original data when measuring the aluminum plate

From the graph, it is apparent that the calibration method corrected the temperature measured by the device, resulting in an average percent error of only 0.43% for the 4.5 hour duration of testing.

To verify that this calibration factor is valid for all temperatures, several tests at different temperatures were performed. In a random order, temperatures in the range of 33.5°C to 41.5 °C were acquired from the aluminum plate in increments of 0.5 °C. Sampled 100 times at each temperature, the average values and standard deviations were calculated and plot in Figure 23.

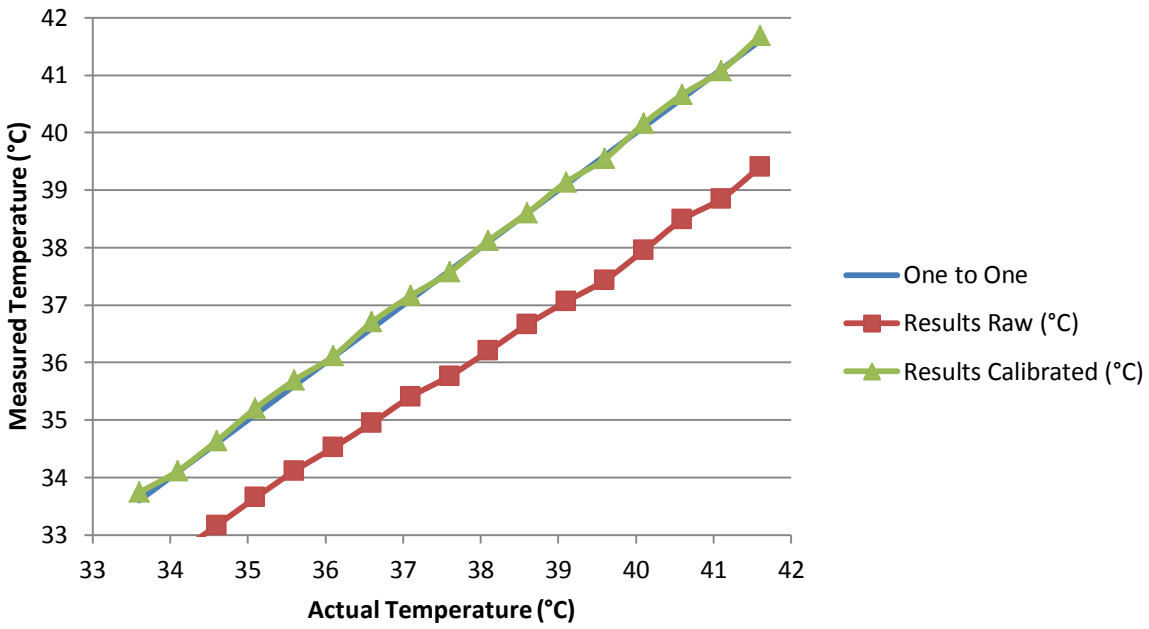

Figure 23: Raw and calibrated (adjusted with calibration factor of 0.79) temperatures detected by the sensor in comparison to the aluminum plate temperature at a variety of different temperatures

From the results, it is verified that the calibration factor used is appropriate for the system at all temperatures in the range the human body operates. With less than a 0.25% error at all temperatures, this device meets the medical standard requiring less than 0.6% error [17].

All of the above tests were run at a constant distance (3.0 mm) from the aluminum calibration plate. To test the consistency at different ranges of the device, the aluminum plate was set to a temperature of 39.1 °C and data acquired at different distances. The uncalibrated results from this test can be seen in Figure 24.

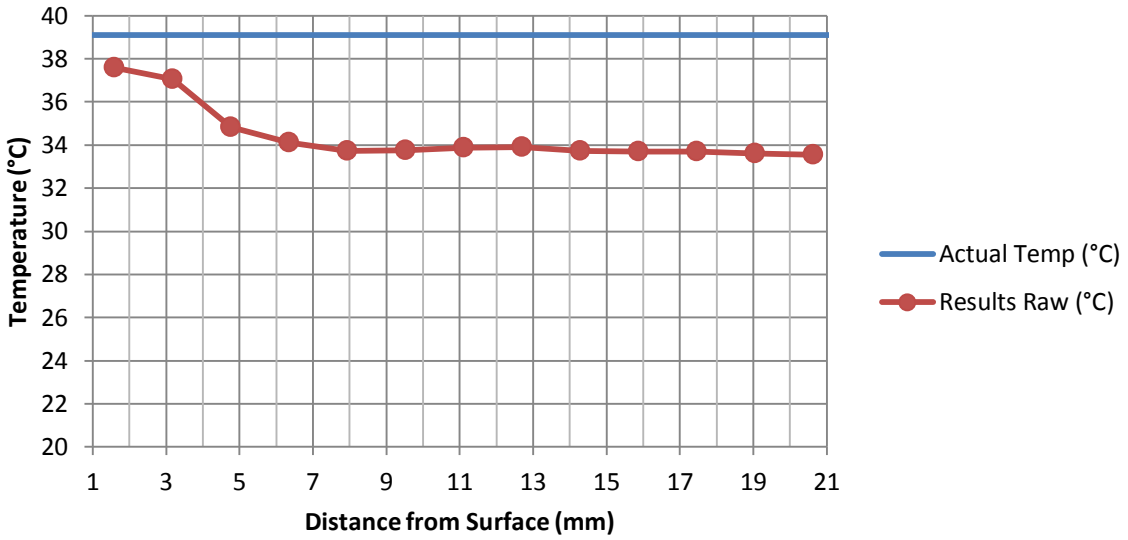

Figure 24: Results measured by the device at different increments while measuring a temperature of 39.1 °C

It is noticed that at low distances, the device estimates larger temperatures. This measured temperature then begins to drop until it is 7 mm away from the surface. After 7 mm it remains constant, for distances tested up to 20 mm. Based on these results, it is apparent that a different calibration factor must be applied depending on the distance of the IR sensor from the highly emissive surface. From the data above, equation 23 was generated to determine calibration factor as a function of distance when measuring a surface with an emissivity of 0.98.

$$F = \begin{cases} 0.0104 * x^3 - 0.1133 * x^2 + 0.3133 * x + 0.58 & , \ x < 6.5\ mm \\ 0.61 & , \ x \geq 6.5 mm \end{cases} \quad (23)$$

where F is the calibration factor and x is the distance the sensor is from the surface in mm. In Table 2 below, the calibration factors for several distances are defined.

Table 2: Calibration factors for the different distances the IR sensor is from the aluminum plate

Distance (mm)	1.5	3	4.5	6	6.5 and greater
Calibration Factor	0.83	0.79	0.64	0.66	0.61

In order to determine if this will have the same effect when implemented in the human ear, further tests involving human subjects must be performed.

To verify that the IR sensor is working properly, a test was performed in which the IR sensor was allowed to cool to room temperature before being placed on the blackbody plate at 41.5 °C. Here, the system response can be observed as the sensor temperature increases from the

heat of the aluminum plate. This will verify that the temperature referencing of the thermistor is working properly. This test was ran twice, at both a close distance (1.5 mm) as well as a further distance (8 mm) to test both the response of the sensor as well as the effectiveness of the calibration factor values. The graphs from these tests can be seen below in Figures 25 and 26.

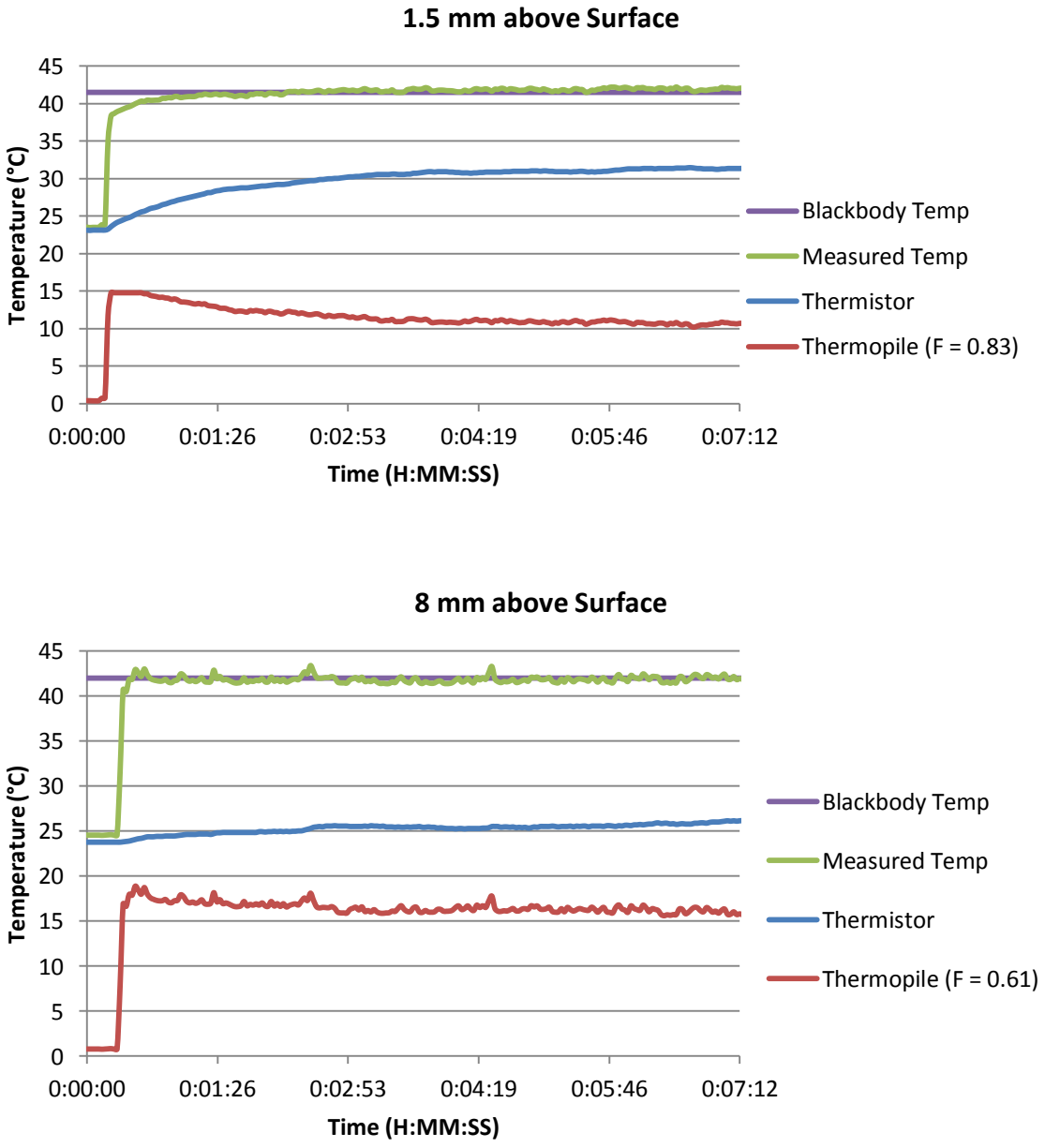

Figure 25 and Figure 26: IR sensor system response showing the outputs of the thermistor and thermopile (adjusted) as the sensor is exposed to the blackbody plate at 41.5 °C at both a 1.5 mm distance and 8 mm distance and adjusted with a calibration factor of 0.83 and 0.61 respectively

At approximately the 14 second mark, the large spike in temperature indicates that the IR is now being exposed to the blackbody plate. Notice how the thermopile immediately detects the large temperature change between the sensor and the surface. After exposure, the device

begins to heat up, as indicated by the rising thermistor temperature. As the device heats up, the difference in temperature between the sensor and the surface decreases, which is indicated by the decreasing thermopile temperature. This proportional response between the thermistor and thermopile validates that the sensor is behaving as expected. It can be seen that when the IR sensor was placed further from the surface does not heat up as much as when it is placed near the sensor. In addition, it is verified that the calibration factors defined work accurately for the tested range of distances.

When the device is being used in the field, the emissivity of skin will have no effect on the results. When inserted into the ear, the sensor on the device will be facing the ear canal as seen in Figure 27.

Figure 27: Diagram of current device design implemented with a human ear

Since the area of the sensor is significantly smaller than the area of the ear canal, the inner ear can be modeled as a cavity. Cavities of any material can be declared as a blackbody from the premise that all radiation emitted inside the cavity will reflect off the cavity walls before reaching the opening, where all radiation and irradiation will be absorbed. Since the inner ear can be modeled as a blackbody, a calibration factor may not be necessary. Further testing involving human subjects will be performed to investigate how these effects will influence the final product.

4.3 RSSI

To develop a relationship between RSSI and proximity a test matrix was devised where the RSSI value would be recorded at set distances in the range of 0 to 100 meters. At each distance, the RSSI between an XBee module and the coordinator was recorded for no interference as well as when a human subject is in the line of sight (LoS). Both scenarios were recorded five times each. The results of these tests can be seen in Figure 28.

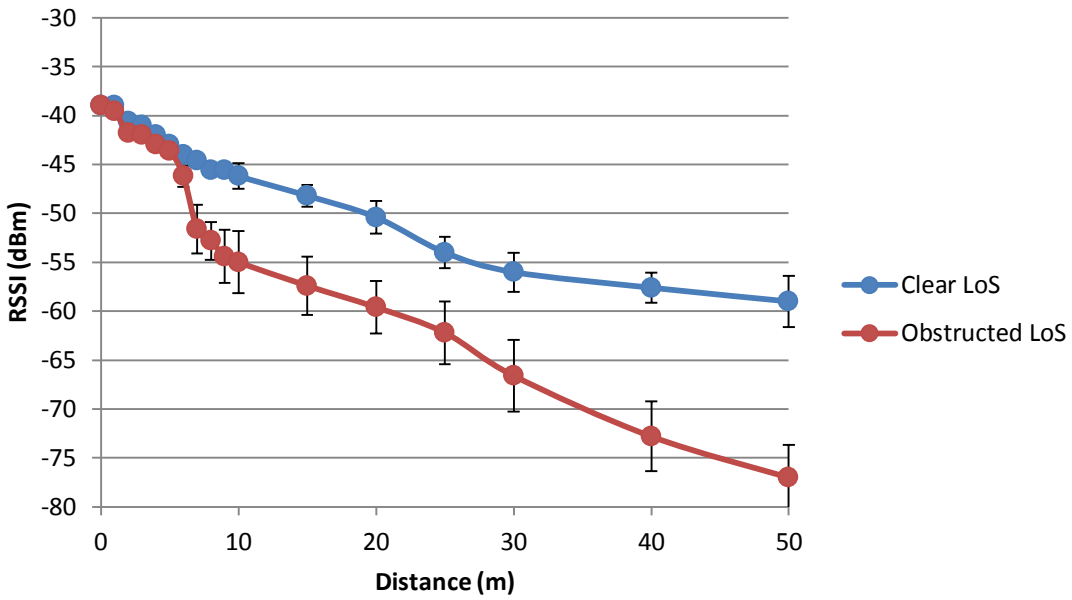

Figure 28: Relationship of RSSI to distance for clear both clear and obstructed line of sight

From the test, it is apparent that there is an inverse relationship between RSSI and the proximity of the XBee module from the coordinator. For close proximities (less than 10 meters), there is a 0.8 dBm/m resolution for RSSI. Since the device can detect RSSI changes in intervals of 1 dBm, the position can be determined within 1.25 meters at these close range distances. At further ranges, the resolution decreases greatly. Since the project is only concerned with close proximity detection, the low resolution in large distances will not be a problem with the systems performance.

5 Conclusion

At this stage, the device is ready to be implemented in the lawn care and agriculture environment. Each worker being monitored will possess a device consisting of the XBee module, the signal conditioning board, the IR temperature sensor, and a battery. The subject will attach the IR sensor to their ear (whichever is preferred) and turn on the device. The ConnectPort X4 modem and a computer with networking capabilities will be placed onboard the lawnmower or tractor in the field. The vehicle's battery will supply power to the modem and computer. The computer will establish a Telnet with the modem via Ethernet connection. After the Telnet is established and the program has begun to execute, the driver of the vehicle will be able to monitor his/her proximity to all workers as well as their core body temperature. Noticeable warnings will be displayed on the computer screen, being observed by the vehicle's driver, when the proximity is breached or a subject's core body temperature rises above the critical temperature. The proximity threshold and critical core body temperature can be set to any desired value.

The ability for the device to accurately measure temperature and determine proximity with the coordinator was verified with the tests performed. It was shown that the XBee modules are capable of successfully acquiring data. By submerging a thermistor into water at 36.5 °C recording the outputs with the XBee module, it was found that the system had a time constant of 0.97 seconds. When compared with the computer model's predicted time constant of 0.71, it was validated that the XBee is able to detect the response to the system in a predictable and prompt manner.

Tests on an aluminum plate coated with an enamel comprising of an emissivity of 0.98, showed that the infrared temperature sensor could estimate a surface temperature with only a 0.43% error. In addition, the proximity sensing using RSSI was able to measure within 1.25 meters of actual location at distances below 10 meters. These test results show that the constructed device can adequately sense core body temperature and proximity using non-invasive measurement techniques.

6 Future Work

At the time of this thesis's submission, approval for human testing was pending approval from the Institutional Review Board (IRB). After approved this test will extend beyond lab tests and include data from human subjects undergoing physical activities. The plan is to have the subject wear the device, while performing a physical activity (i.e. jogging or biking) for a maximum of 20 minutes. Throughout the test, core body temperature and proximity will be recorded from the system developed in this thesis and analyzed. These recorded values will be compared with temperatures recorded using medical grade thermometers and premeasured distance markers, to supply a final verification that the device performs to an acceptable accuracy.

Enhancements to the system could be made to make the interface more user friendly. First, a more advance form of outputting the information can be made, involving charts and colors rather than only text. This could reduce the effort required for the supervisor to monitor the several workers he/she is responsible for as well as eliminate the necessity of a computer in the system. The coding can also go on to turn off the engine of the lawnmower/tractor in the event of a proximity breach. This would work similar to the safety switch under new lawn mowers, which turns the engine off when it detects no driver is present. Enhancements to the wearable device could also be made. By adding a speaker and LEDs to the device, the wearer could also be warned of any dangers, in addition to the supervisor. This would increase the awareness and probability that any warnings will be promptly noticed and responded to.

Lastly, a fully designed enclosure for the device and an improved earplug could be developed. Making the device more ergonomic for the customer would make the device more desirable for the end user.

7 Bibliography

1. NIOSH/CDC, *Injuries Among Youth on Farms, 2001.* National Institute for Occupational Safety and Health, 2004. **Publication No. 2004-172**.

2. Bouchama, A. and J.P. Knochel, *Heat stroke.* N Engl J Med, 2002. **346**(25): p. 1978-88.

3. Argaud, L., et al., *Short- and long-term outcomes of heatstroke following the 2003 heat wave in Lyon, France.* Arch Intern Med, 2007. **167**(20): p. 2177-83.

4. Leon, L.R. and B.G. Helwig, *Heat stroke: role of the systemic inflammatory response.* J Appl Physiol, 2010. **109**(6): p. 1980-8.

5. Kakitsuba, N., I.B. Mekjavic, and T. Katsuura, *Individual variability in the core interthreshold zone as related to body physique, somatotype, and physical constitution.* J Physiol Anthropol, 2009. **28**(6): p. 275-81.

6. WebMD. *Body Temperature*. First Aid & Emergencies 2011; Available from: http://firstaid.webmd.com/body-temperature.

7. Leon, L.R. and B.G. Helwig, *Heat Stroke: Role of the Systemic Inflammatory Response.* J Appl Physiol, 2010.

8. Nybo, L., *Exercise and heat stress: cerebral challenges and consequences*, 2007, Elsevier. p. 29-43.

9. Glazer, J.L., *Management of Heatstroke and Heat Exhaustion.* American Family Physician, 2005. **71**(11): p. 2133-2140.

10. Hall, D.M., et al., *Mechanisms of circulatory and intestinal barrier dysfunction during whole body hyperthermia.* Am J Physiol Heart Circ Physiol, 2001. **280**(2): p. H509-21.

11. Gierckskey, T., et al., *Severe liver failure in exertional heat stroke.* Scand J Gastroenterol, 1999. **34**(8): p. 824-7.

12. Mustafa, K.Y., et al., *Blood coagulation and fibrinolysis in heat stroke.* Br J Haematol, 1985. **61**(3): p. 517-23.

13. O'Kane, B.L., et al., *Dynamics of Human Thermal Signatures.* InfraMation, 2004.

14. Hayashi, K., et al., *Relationship between ventilatory response and body temperature during prolonged submaximal exercise.* J Appl Physiol, 2006. **100**(2): p. 414-20.

15. Gonzalez-Alonso, J., et al., *Influence of body temperature on the development of fatigue during prolonged exercise in the heat.* J Appl Physiol, 1999. **86**(3): p. 1032-9.

16. Astrand, P.O. and B. Saltin, *Maximal oxygen uptake and heart rate in various types of muscular activity.* J Appl Physiol, 1961. **16**: p. 977-81.

17. Casa, D.J., et al., *Validity of devices that assess body temperature during outdoor exercise in the heat.* J Athl Train, 2007. **42**(3): p. 333-42.

18. Agilent *Practical Temperature Measurements*. Application Note 290, 2009.

19. Liew, D.S.C. *Electromagnetic Waves*. [cited 2011 September 8, 2011].

20. Howell, J.R., R. Siegel, and M.P. Mengüç, *Thermal radiation heat transfer*. 5th ed2011, Boca Raton: CRC Press. xxx, 957 p.

21. PerkinElmer, I., *Thermoelectric Infrared Sensors (Thermopiles) for Remote Temperature Measurements; Pyrometry.* 2006.

22. Incropera, F.P., *Fundamentals of heat and mass transfer*. 6th ed2007, Hoboken, NJ: John Wiley. xxv, 997 p.

23. *Emissivity Values for Common Materials*. [cited 2011 October, 26]; Available from: http://infrared-thermography.com/material-1.htm.

24. LaserTechnik, R., *Thermopile Infrared Sensor.*

25. DigiInternational, *http://www.digi.com/*: 11001 Bren Road East, Minnetonka, MN 55343.

26. Surgeons, A.S.o.P., *Lawn Mowing Injuries Common In Children And Teens.* ScienceDaily, 2008.

27. Clemmensen, J.S., *Design of a Control System for Multiple Autonomous Ground Vehicles to Achieve a Self Deployable Security Perimeter.* 2007.

28. Wolfram, *Mathematica*: Wolfram Research, Inc.

29. PerkinElmer, I., *http://www.perkinelmer.com/*: 940 Winter Street, Waltham, Massachusetts 02451.

30. PerkinElmer, I., *TPS 333 - Thermopile Detector.* Optoelectronics, 2003.

31. TexasInstruments, *Precision, Low Power INSTRUMENTATION AMPLIFIERS.* Burr-Brown Products, 2005.

32. CadSoft, *Easily Applicable Graphical Layout Editor (EAGLE)*.

33. Eclipse, *Digi ESP for Python*, DigiInternational, Editor.

8 Appendix A: Thermistor Computer Model

The following Mathematica code was developed and used to model the thermistor's temperature response when submerged into water.

First, all values used are cleared to prevent errors in the code from run to run.

```
Clear[T,Tf,To,SettlingTemp,t,TempWater,ThermEnergyBalWater,EnGenTherm,qCondWater
,i,V,Diameter,SATherm,k,h,TempH2O]
```

Next, all the properties of the thermistor are defined.

Properties of Thermistor

```
ρ=850;
Cp=500;
∈=.89;
i=27.01*10^(-6);
V=0.5989;
Diameter=0.0024;
SATherm=7.2*10^(-5);
Vol=(4/3)Pi*(.0024/2)^3;
```

Then the properties of water are defined.

Properties of Water

```
h=100;
Tc=36.5;
qConvWater[T_,Tc_]:=SATherm*h(Tc-T);
EnGenTherm=i*V;
```

Finally, using conduction and convection energy equations, the bulk of the code solves the differential equations over time and plots the predicted response of the system.

Energy Balance Equations

```
ThermEnergyBalWater[T_,Tc_]:=qConvWater[T,Tc]+EnGenTherm;

SettlingTemp=Solve[ThermEnergyBalWater[T,Tc]==0,T]

Tc=T/.SettlingTemp;

To=24.0556;

TempFunc[To_,Tc_,tmax_]:=
 NDSolve[
  {
   ThermEnergyBalWater[T[t],Tc]==ρ*Vol*Cp*T'[t],
   T[0]==To
```

```
  },
 T,
 {t,0,tmax}]

TempFuncPlot[To_,Tc_,tmax_]:=
 Plot[
  Evaluate[T[t]/.TempFunc[To,Tc,tmax]],
  {t,0,tmax},
  PlotRange→{To-3,Tc+3},
  AxesLabel→{"Time(s)","Temperature(℃)"}]

TempFuncPlot[25,36.5556,5]
```

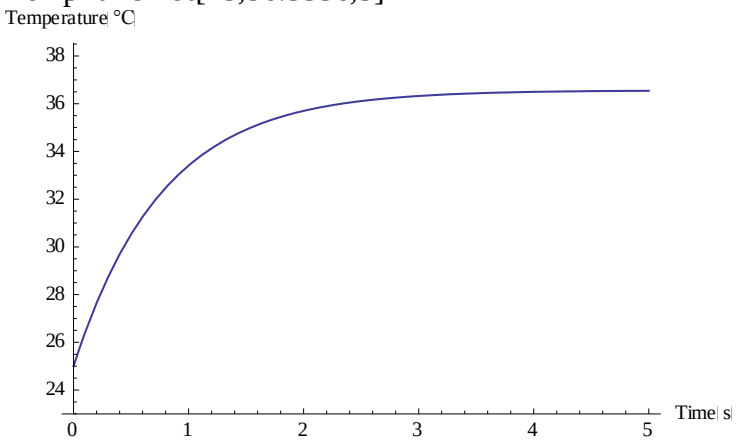

9 Appendix B: Eagle PCB Model

Several steps were taken to create a PCB of the IR sensor signal conditioner. Using the EAGLE CAD program, first the schematic was created as seen in Figure B- 1.

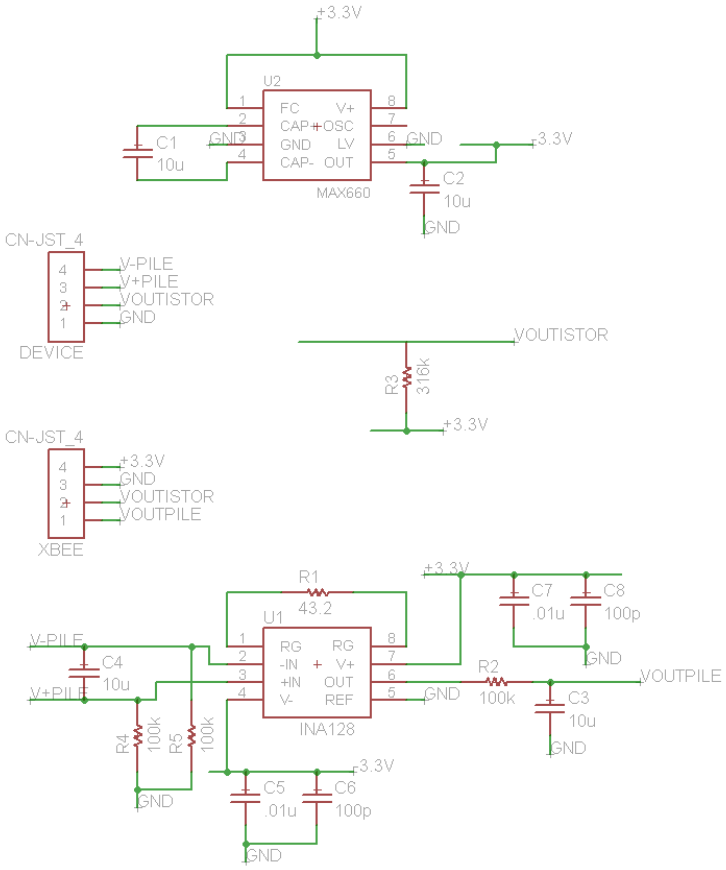

Figure B- 1: Schematic of IR sensor signal conditioner

A MAX660 was included in the circuit to regulate the 3.3 V supplied by the XBee module and also create a -3.3 V output. The 3.3 V and -3.3 V nodes are used to power the INA128 In-Amp and the thermistor. After the schematic was created, checked, and verified, a board was created, seen in Figure B- 2.

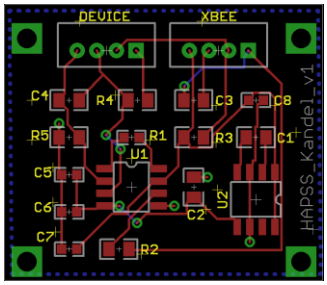

Figure B- 2: Virtual board of IR sensor signal conditioner

Optimized to the smallest possible area, 5 resistors, 8 capacitors, 2 integrated circuits, and 2 JST connecters were arranged and labeled on the board. Again, the board was checked and verified.

Next, the board was sent to a PCB manufacturer who checked the board for any sources of errors and returned the finished design. What was returned held no components, as the manufacturer only created the PCB seen in Figure B- 3. For this reason, it was important to label all components to be placed on the board.

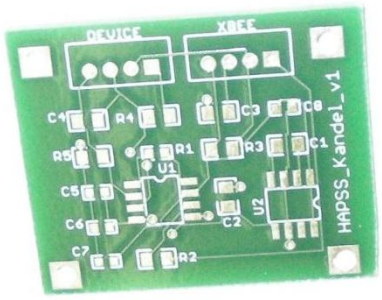

Figure B- 3: PCB of IR sensor signal condition before popularized with components

From a separate vender, the components were ordered and soldered to the PCB. The finished PCB is seen in Figure B- 4.

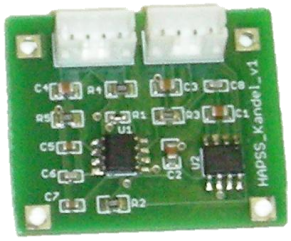

Figure B- 4: Printed Circuit Board containing all elements of the thermopile and thermistor circuits

10 Appendix C: Python Code

The python code consists of three separate files. The master file is the snsorlt.py file, and while running its process calls the xbeelt.py and xbeelt2.py files. The three files are seen below.

sensorlt.py:

```
################################################################################
####    Define and import required libraries                    ####
################################################################################

import sys, os
import libs.xbeelt
import libs.xbeelt2
import time
import zigbee, struct
import math
#import winsound,sys


################################################################################
####    Define the XBee modules' MAC addresses                  ####
################################################################################

sensor_addresses = [
#               "[00:13:a2:00:40:62:d6:98]!"
#               "[00:13:a2:00:40:62:ce:24]!"
              "[00:13:a2:00:40:62:ce:27]!"
              ]

number_devices = len(sensor_addresses)


################################################################################
####    Set the critical condition values                       ####
################################################################################

temp_crit = 78     #Prints warning for temperatures above this value
rssi_crit = 40     #Prints warning for RSSI below this value


################################################################################
####    Set conditions determining duration of data acquisition     ####
################################################################################
t=1

while t<400:       # Loop will run while values are "True"


################################################################################
####    Calls XBee Modules to receive infromation               ####
################################################################################

   n=0          #Resets "n" before sampling all devices
```

```
#    print
'\r\n\r\n\r\n\r\n\r\n\r\n\r\n\r\n\r\n\r\n\r\n\r\n\r\n\r\n\r\n\r\n\r\n\r\n============================================
=='

    while (number_devices - n > 0):

        """Retrieve voltage value from Thermistor"""
        sensor = libs.xbeelt.XBeeLTN(sensor_addresses[n])
        sample = sensor.sample()
        mVThermistor=sample['voltage']
        VThermistor=mVThermistor/1000.0

#        print "\rThermistor:    %s V" %(VThermistor)

        """Retrieve voltage value from Thermopile"""
        sensor = libs.xbeelt2.XBeeLTN(sensor_addresses[n])
        sample = sensor.sample()
        mVThermopile_amplified=sample['voltage']
        mVThermopile=(mVThermopile_amplified/1220.0)

#        print "\rThermopile:    %s V" %(mVThermopile_amplified/1000.0)

        """Receive the supply voltage from the device"""
        vcc_raw = zigbee.ddo_get_param(sensor_addresses[n], '%V')
            #Collect the raw Vcc info from the packet
        vcc_hex = "0x%s" % ''.join( [ "%02X" % ord( x ) for x in vcc_raw ] ).strip()
            #Decifer the value into a hexidecimal value
        vcc_dec = int(vcc_hex, 16)
            #Convert the hexidecimal value into an integer
        vcc_v = vcc_dec * 1.200 / 1024.0
            #Conversion factor for the system from datasheet

        """Convert Thermistor voltage into resistance"""
        res_Thermistor = (VThermistor*316000.0)/(vcc_v-VThermistor)

        """Derive Thermistor temperature from resistance """
        temp_Thermistor_r = 3964.0/(math.log(res_Thermistor/0.168235))
        temp_Thermistor_c = temp_Thermistor_r - 273.15
        temp_Thermistor_f = temp_Thermistor_c*1.8+32.0

#        print "\rThermistor Temp:    %s C" %(temp_Thermistor_c)

        """Convert Thermopile voltage into temperature"""
        temp_Thermopile_c = -0.032*math.pow(mVThermopile,4) + 0.2127*math.pow(mVThermopile,3) -
1.0442*math.pow(mVThermopile,2) + 14.292*mVThermopile + 0.1094
        temp_Thermopile_f = temp_Thermopile_c*1.8

#        print "\rThermopile Temp:    %s C" %(temp_Thermopile_c)
#
#
        """Rounds selected temperature for output"""
        temp_adjusted = temp_Thermistor_c + temp_Thermopile_c
        temp_out = round(temp_adjusted,5)

        """Retrieve RSSI values from module"""
        rssi_raw = zigbee.ddo_get_param(sensor_addresses[n], 'DB')      # Returns string for RSSI
        rssi_val_tuple = struct.unpack('=B', rssi_raw)                  # Unpacks string into tuple
        rssi_val_int = rssi_val_tuple[0]                                # Converts tuple into int
```

```
        """Print values and warnings"""
#       print '\r\nDevice', n+1
#       print "\r\nTemperature:    %s C" %(temp_out)                  # Prints temp_pro
        print temp_Thermistor_c
        print temp_Thermopile_c
        print temp_out
#       if temp_out > temp_crit:                                  # Compares temp_pro to critical condition
#           print 'TEMPERATURE ALERT'                                 # Prints warning if conditions exceed critical
#       print 'RSSI:         -', rssi_val_int, ' dBm'                # Prints RSSI
#       if (rssi_val_int < 40):                                   # Compares RSSI to critical condition
#           print 'PROXIMITY ALERT'                                   # Prints warning if conditions exceed critical

        n=n+1

    print time.ctime()
#   print '\r\n============================================='
    time.sleep(60)
    t=t+1
```

xbeelt.py:

```
import xbee as zigbee
from xbeeprodid import *
from xbeedevice import *
from sensor_io import parseIS
import math
import zigbee, struct

class XBeeLTN(XBeeDevice):
    """XBeeLTN - object representing a an XBee LT device on the mesh.
    This object allows the configuration and use of an XBee LT device."""


    def __init__(self, addr):
        """addr - IEEE 802.15.4 address of XBee LT Adapter module."""

        XBeeDevice.__init__(self, addr)
        """Verify that device is truly a LT Adapter"""
#       print "Product type: %s" %self.product_type
#       print "SelnsorLT type: %s" %XBeeSensorLTAdapter
#       if self.product_type != XBeeSensorLTAdapter:
#           raise ValueError, "Adapter is not a %s" % (GetXBeeProductName(XBeeSensorLTAdapter))

        """The XBee needs to have analog IO 1 and 2 (pins 19, 18) set to 'ADC'"""
        self.XBeeCommandSet("d1", 2)
        self.XBeeCommandSet("d2", 2)
        self.XBeeCommandSet("wr", "")
        self.XBeeCommandSet("ac", "")



    def raw_sample(self, io_sample=None):
        """raw_sample(channel) => A/D reading
        Returns raw unscaled A/D light and temperature sample data"""

        if io_sample is None:
          io_sample = self.XBeeCommandGet("is")
```

```
#       light = parseIS(io_sample)["AI1"]
        temp  = parseIS(io_sample)['AI1']

        item = {'voltage': temp}
        return item

    def sample(self, io_sample=None):
        """sample() => Converts raw sensor data into actual usable values."""
        item = self.raw_sample(io_sample)

        """Receive the analog voltage from the devices"""
        mVolts = (float(item['voltage'])/1023.0)*1200.0


        """Returns voltage value"""
        item = { 'voltage': mVolts}


        return item
```

xbeelt2.py:

```
import xbee as zigbee
from xbeeprodid import *
from xbeedevice import *
from sensor_io import parseIS
import math
import zigbee, struct

class XBeeLTN(XBeeDevice):
    """XBeeLTN - object representing a an XBee LT device on the mesh.
    This object allows the configuration and use of an XBee LT device."""


    def __init__(self, addr):
        """addr - IEEE 802.15.4 address of XBee LT Adapter module."""

        XBeeDevice.__init__(self, addr)
        """Verify that device is truly a LT Adapter"""
#       print "Product type: %s" %self.product_type
#       print "SelnsorLT type: %s" %XBeeSensorLTAdapter
#       if self.product_type != XBeeSensorLTAdapter:
#           raise ValueError, "Adapter is not a %s" % (GetXBeeProductName(XBeeSensorLTAdapter))

        """The XBee needs to have analog IO 1 and 2 (pins 19, 18) set to 'ADC'"""
        self.XBeeCommandSet("d1", 2)
        self.XBeeCommandSet("d2", 2)
        self.XBeeCommandSet("wr", "")
        self.XBeeCommandSet("ac", "")



    def raw_sample(self, io_sample=None):
        """raw_sample(channel) => A/D reading
        Returns raw unscaled A/D light and temperature sample data"""

        if io_sample is None:
```

```
        io_sample = self.XBeeCommandGet("is")

#       light = parseIS(io_sample)["AI1"]
        temp  = parseIS(io_sample)["AI2"]

        item = {'voltage': temp}
        return item

    def sample(self, io_sample=None):
        """sample() => Converts raw sensor data into actual usable values."""
        item = self.raw_sample(io_sample)

        """Receive the analog voltage from the devices"""
        mVolts = (float(item['voltage'])/1023.0)*1200.0


        """Returns voltage value"""
        item = { 'voltage': mVolts}


        return item
```

11 Appendix D: IR Sensor Radiosity Model

By developing a model to characterize the elements of heat-transfer occurring, the sensor will need to be calibrated to account for the effects. The model, seen in Figure D- 1, shows the orientation in which the test was administered and the sources of radiation.

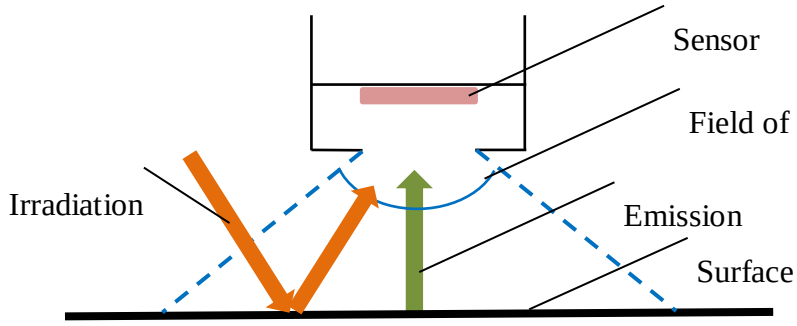

Figure D- 1: Model of setup for the testing of the IR sensor with the aluminum plate

With the ambient room, there is a significant area on the surface in which irradiation can reflect, and be misinterpreted by the sensor. To characterize this effect, the radiosity, sum of reflected and emitted radiation, of the surface is derived in equation D-1:

$$J = \varepsilon E_{b,surface} + \rho G \qquad \text{(D- 1)}$$

where J is the radiosity of the surface, ε is the emissivity of the surface, $E_{b,surface}$ is the blackbody emissive power of the surface, ρ is the reflectivity of the surface, and G is the irradiation from the room. To make this equation specific to the test setup used, the following relationships are declared. First, blackbody emissive power is defined as:

$$E_b = \sigma T_{surface}^4 \qquad \text{(D- 2)}$$

where σ is the Boltzmann constant. Next, reflectivity is defined as:

$$\rho = 1 - \varepsilon \qquad \text{(D- 3)}$$

where ε is the emissivity of the surface. Lastly, the room is classified as a blackbody and defines the irradiation from the room as:

$$G = E_{b,room} \qquad \text{(D- 4)}$$

where $E_{b,room}$ is the blackbody emissive power of the room. Using these definitions, equation D-1 can rewritten as:

$$J = \varepsilon\sigma T_{surface}^4 + (1-\varepsilon)E_{b,room} \quad \text{(D- 5)}$$

Next, the heat flux equation of the sensor is defined in terms of energy into the sensor and energy out of the sensor in equation D-6:

$$q" = F * J - F * E_{b,sensor} = F\left[J - E_{b,sensor}\right] \quad \text{(D- 6)}$$

where *q"* is the heat flux of the sensor, *J* is the radiosity of the surface, and $E_{b,sensor}$ is the blackbody emissive power of the sensor. A calibration factor, *F*, is also added to the equation and will be derived experimentally in the lab. It should be noted that the radiosity of the surface accounts for the energy going into the sensor and the emissive power of the sensor accounts for energy leaving the sensor. When equation D-5 is substituted into equation D-6 the following equation is derived:

$$q" = F\left[\varepsilon\sigma T_{surface}^4 + (1-\varepsilon)E_{b,room} - E_{b,sensor}\right] \quad \text{(D- 7)}$$

To simplify this expression further, the assumption must be made that the temperature of the sensor is the same as the temperature of the room. After making this assumption, the equation reduces to:

$$q" = F * \varepsilon\left[\sigma T_{surface}^4 - E_{b,sensor}\right] = F * \varepsilon\left[\sigma T_{surface}^4 - \sigma T_{sensor}^4\right] \quad \text{(D- 8)}$$

Since ΔT is the primary focus, it can be declared that:

$$\Delta T \sim {q"}/{F * \varepsilon} \sim {q"}/{F} \quad \text{(D- 9)}$$

where *q"* is the heat flux of the sensor, which is measured by the thermopile. From this method, it can be derived that the heat flux measured by the sensor must be divided by a calibration factor, derived experimentally. The calibration factor will account for emissivity, field of view, and irradiation from the environment.

12 Appendix E: IRB Approval Letter

VirginiaTech

Office of Research Compliance
Institutional Review Board
2000 Kraft Drive, Suite 2000 (0497)
Blacksburg, Virginia 24060
540/231-4606 Fax 540/231-0959
e-mail irb@vt.edu
Website: www.irb.vt.edu

MEMORANDUM

DATE: December 5, 2011

TO: Robert D. Grisso, Matthew Kreisman Kandel

FROM: Virginia Tech Institutional Review Board (FWA00000572, expires May 31, 2014)

PROTOCOL TITLE: YSILC

IRB NUMBER: 11-1032

Effective December 5, 2011, the Virginia Tech IRB Chair, Dr. David M. Moore, approved the new protocol for the above-mentioned research protocol.

This approval provides permission to begin the human subject activities outlined in the IRB-approved protocol and supporting documents.

Plans to deviate from the approved protocol and/or supporting documents must be submitted to the IRB as an amendment request and approved by the IRB prior to the implementation of any changes, regardless of how minor, except where necessary to eliminate apparent immediate hazards to the subjects. Report promptly to the IRB any injuries or other unanticipated or adverse events involving risks or harms to human research subjects or others.

All investigators (listed above) are required to comply with the researcher requirements outlined at http://www.irb.vt.edu/pages/responsibilities.htm (please review before the commencement of your research).

PROTOCOL INFORMATION:
Approved as: **Expedited, under 45 CFR 46.110 category(ies) 4, 7**
Protocol Approval Date: **12/5/2011**
Protocol Expiration Date: **12/4/2012**
Continuing Review Due Date*: **11/20/2012**
*Date a Continuing Review application is due to the IRB office if human subject activities covered under this protocol, including data analysis, are to continue beyond the Protocol Expiration Date.

FEDERALLY FUNDED RESEARCH REQUIREMENTS:
Per federally regulations, 45 CFR 46.103(f), the IRB is required to compare all federally funded grant proposals / work statements to the IRB protocol(s) which cover the human research activities included in the proposal / work statement before funds are released. Note that this requirement does not apply to Exempt and Interim IRB protocols, or grants for which VT is not the primary awardee.

The table on the following page indicates whether grant proposals are related to this IRB protocol, and which of the listed proposals, if any, have been compared to this IRB protocol, if required.

Date*	OSP Number	Sponsor	Grant Comparison Conducted?

*Date this proposal number was compared, assessed as not requiring comparison, or comparison information was revised.

If this IRB protocol is to cover any other grant proposals, please contact the IRB office (irbadmin@vt.edu) immediately.

cc: File

13 Appendix F: IRB Consent Form

YOUTH SAFETY IN LAWN CARE SENSOR BASED TEST

INFORMATION SHEET FOR

PARTICIPANTS

Thank you for showing an interest in this project. Please read this information sheet carefully before deciding whether or not to participate. If you decide to participate we thank you. If you decide not to take part there will be no disadvantage to you of any kind and we thank you for considering our request.

Project Reasoning

The project, devised by the Virginia Cooperative Extension, was formed to develop a non-intrusive sensor based device that is capable of monitoring core body temperature and proximity of a subject. This project is being undertaken as part of the requirements for the Postgraduate Diploma in Science.

The goal of the project is to develop a device that can reliably monitor the core temperature subjects utilizing the device as well as their proximity to the coordinator. The final application will be used to monitor youth workers in the agriculture and lawn care industries.

Participant Qualification

This project seeks males and females above the age of 18 who are capable of extended physical exertion.

People who are in one or more of the categories listed below will not be able to participate in the project because, in the opinion of the researchers and the Ethics Committee of the University, it may involve an unacceptable risk to them:-

- Suffer from heart conditions
- Diagnosed with severe asthma
- Expectant mothers
- Incapable of extended physical activity

Participant Duties

Should you agree to take part in this project, you will be asked to exercise a physically demanding exercise (i.e. jogging or biking) for no longer than a 20 minute period, while wearing the device constructed by the research team. The device will be attached to the waist of the participant with an ear-plug sensor inserted into the ear. The participant may choose which ear the device is to be worn.

Although the device was ergonomically designed to be non-intrusive, participants may find a slight discomfort from the device.

Please be aware that you may decide not to take part in the project without any disadvantage to yourself of any kind.

Participant Withdrawal

You may withdraw from participation in the project at any time and without any disadvantage to yourself of any kind.

Virginia Tech Institutional Review Board Project No. 11-1032
Approved December 5, 2011 to December 4, 2012

Data Collected

A record of core body temperature and proximity data will be collected throughout the testing duration.

The data collected will be used to verify the accuracy of the developed device.

Results of this project may be published but any data included will in no way be linked to any specific participant.

You are most welcome to request a copy of the results of the project should you wish.

The data collected will be securely stored in such a way that only the project team will be able to gain access to it. At the end of the project any personal information will be destroyed immediately except that, as required by the University's research policy, any raw data on which the results of the project depend will be retained in secure storage for five years, after which it will be destroyed.

Question From the Participant

If you have any questions about our project, either now or in the future, please feel free to contact either:-

Matthew Kandel	or	Dr. Robert Grisso
Dept. of Mechanical Engineering		Dept. of Biological Systems Engineering
mkandel@vt.edu		rgrisso@vt.edu

This project has been reviewed and approved by the Ethics Committee

of the Virginia Tech University IRB

Virginia Tech Institutional Review Board Project No. 11-1032
Approved December 5, 2011 to December 4, 2012

YOUTH SAFETY IN LAWN CARE SENSOR BASED TEST

CONSENT FORM FOR

PARTICIPANTS

I have read the Information Sheet concerning this project and understand what it is about. All my questions have been answered to my satisfaction. I understand that I am free to request further information at any stage.

I know that:-

1. my participation in the project is entirely voluntary;

2. I am free to withdraw from the project at any time without any disadvantage;

3. the data will be destroyed at the conclusion of the project but any raw data on which the results of the project depend will be retained in secure storage for five years, after which it will be destroyed;

4. slight discomfort may arise;

5. the results of the project may be published but my anonymity will be preserved.

I agree to take part in this project.

....

(Signature of participant) (Date)

This project has been reviewed and approved by the Ethics Committee

of the Virginia Tech University IRB

Virginia Tech Institutional Review Board Project No. 11-1032
Approved December 5, 2011 to December 4, 2012

14 Appendix G: Letters of Permission for Copyright Material

From: Orlove, Gary <Gary.Orlove@flir.com>
Sent: Tuesday, December 06, 2011 10:08 AM
To: mkandel@vt.edu
Subject: RE: Request

Matthew,

Please feel free to use the image. Please credit as

"O'Kane, Barbara L.; Sandick, Philip; Shaw, Todd; Cook, Michael "Dynamics of human thermal signatures." In Inframation 2004 Proceedings Volume 5, pp 29-38"

Regards,

Gary

Gary Orlove, P.E.
ASNT NDT Level III TIR
BINDT IRT L3-MC, L3-CV
| Program Manager | Application Engineer
| InfraMation Thermography Conference Co-Chairman | www.inframation.org |
| www.infraredtraining.com | 978-901-8245 | gary.orlove@infraredtraining.com

From: Sawyer, Keith
Sent: Thursday, December 01, 2011 4:31 PM
To: Tedford-Tierney, Karen; Loveland, Jennifer
Subject: Request

Email mkandel@vt.edu
First name Matthew
Last name Kandel
Campaign InfraMation Website
Comments:
I would like to include an image from "Dynamics of Human Thermal Signatures" by O'Kane, Sandick, Shaw, and Cook in my thesis. I was wondering if you could grant me permission, or supply me to the correct contact that could.
The article is from 2004.

Thank you,

Keith Sawyer
Inside Sales Manager

FLIR Commercial Systems, Inc.
27700 SW Parkway Avenue

Wilsonville, OR 97070

Direct: 503.498.3840 | Mobile: 503.269.5045
Toll Free 877.773.3547
www.FLIR.com